LIGHT TRAPPING DESIGNS FOR THIN SILICON SOLAR CELLS

by

James Gichuhi Mutitu

A thesis submitted to the Faculty of the University of Delaware in partial fulfillment of the requirements for the degree of Master of Degree in Major

Spring 2010

LIGHT TRAPPING DESIGNS FOR THIN SILICON SOLAR CELLS

by

James Gichuhi Mutitu

Approved: _____
Dennis W. Prather, Ph.D.
Professor in charge of thesis on behalf of the Advisory Committee

Approved: _____
Kenneth E. Barner, Ph.D.
Chair of the Department of Electrical and Computer Engineering

Approved: _____
Michael J. Chajes, Ph.D.
Dean of the College of Engineering

Approved: _____
Debra Hess Norris, M.S.
Vice Provost for Research and Graduate Studies

ACKNOWLEDGMENTS

I first of all want to thank God for His love and grace that have kept me through the years.

My educational journey would not have been possible without the love, care and support of my family to whom I extend my deepest gratitude. Special thanks goes to my Mother Wanjiru for her guidance and my father Mutitu for his strength. I also want to specially thank my cousin Maina for being there when I need him and also, of course, for the legend of Mofat.

I would like to thank Dr. Prather for his vision, enthusiasm and his determination to turn me into philosopher and lover of wisdom; yes we can!, Dr. Barnett for his optimism and vision for a better world; I think some of it has rubbed off on me, Dr. Shouyuan Shi for being available to answer my n^n number of questions; it is always a pleasure to work with you and Dr. Honsberg, for her caring attitude.

I would also like to thank all my co – workers, i.e., members of the Dennis Prather research group and its affiliates and members of the solar power group; it is always a joy to feel accepted in so many different places.

I extend my deepest gratitude to the Department of Electrical and Computer Engineering for being my home. I thank Kathy and Debbie for being available to chat and solve my millions of problems, Pam for all her help, Barbara for keeping her door

open, Christine for all her advice on how to overcome SAD and Kjeld for always being so gracious.

I would also like to thank Dr. Weile for all the humor, Dr. Olowolafe for his kindness, Dr. Cloutier for being available to ask questions, Dr. Hunsperger for all the chats – I hope they come out with a Swahili version of Integrated Optics and Dr. Ih who always says hello. I would also like to extend my thanks to Dr. Appelbaum for the times he actually stood around and joked; yes, there were times.

A special thanks to Dr. Attoh – Okine for being a friend and Dr. Maloba for all the encouragement.

I would like to thank all my friends from all corners of the globe; I feel like a citizen of the world because of all of you.

A special thanks goes to all my childhood friends; Kibe, Kanja, Tony, Kahiga, Thairu, Juliet, Emmanuel, Noel, Gatei, Patricia, Kabui, George Mathenge, Ohawa, Paul Munene, Kevo and the Lang'ats (Beno and Chemu). I can't imagine how life would have been without all of you.

Another special word of thanks goes to Nonie, Gloria, Kristy, Jessie, Ginger, Eric, Ruth and Albert for all being an integral part of my Delaware experience.I also want to thank Mike for all the stunts and Iftekhar for the anti-stunts.

I would also like to thank my friends from Bennington College; Norman Derby for all the help, Susan Sgorbati for being so great, Daniel Michaelson for being great too, Prof. Graves for the encouragement, Hellie for being like family, Jesse Jewel for being ever so helpful and Emilz Rodriguez for being so real.

There are too many people, literally, in my life that I need to thank, so I take this opportunity to thank all the people who have been my friends over the years. It is a pleasure to know you all.

TABLE OF CONTENTS

LIST OF TABLES

LIST OF FIGURES

ABSTRACT

With the increasing scarcity of fossil fuels and a general concern for the environmental impacts of carbon emissions and hazardous radiation, the need for clean renewable energy sources has become not only a national priority but also an issue of national security. Renewed interest in the development of solar electricity has led to the development of new avenues that address the issues of cost and efficiency associated with photovoltaics. One of the prominent approaches being explored is thin film solar cell technology, which offers prospects of lower material costs and increases the adaptability of solar cell design. The goal of this work is to increase the efficiency and versatility of thin film solar cell devices through the development of improved light trapping schemes. Enhanced light trapping schemes increase the absorption of light within solar cell devices and thereby increase the efficiency and ultimately reduce the cost per watt of energy produced.

This thesis introduces the fundamental ideas behind the science of light trapping in thin silicon solar cells. The specific approach involves enhancing the light trapping capabilities, of the thin solar cells, by incorporating photonic device engineering concepts which include photonic crystals, diffraction gratings and antireflective coatings. These concepts are then used to develop novel light trapping designs that are applied to stand alone and multiple junction thin silicon solar cells. The new designs, that are developed, incorporate one dimensional photonic crystals as band pass filters that reflect short light wavelengths (400 – 1100 nm) and transmit longer wavelengths(1100 -1800 nm) at the interface

between two adjacent cells. In addition, nano structured diffraction gratings that cut into the photonic crystal layers are incorporated to redirect incoming waves and hence increase the optical path length of light within the solar cells.

Chapter 1

INTRODUCTION

The issue of clean renewable energy sources has, in recent months, transcended from a subject of importance to researchers and environmentalists to one of national interest that concerns economic progress, the welfare of working families, increasing national security and saving the environment [1]. There has also arisen much concern for the future of the U.S. economy and hence, pressure on the powers that be to map out a path for future technologies that will tackle the rising unemployment gap. To this end, the government proposed its New Energy for America initiative where 'harnessing the power of the sun' [2], was identified as one of the avenues that will champion this endeavor. With this type of interest, there has arisen popular rhetoric surrounding the concept of 'green economics'. As a consequence, photovoltaics have come to be viewed as a saving technology and also as a face for future green economic trends. Hence, it is safe to say that the case for solar electricity has been articulated; at least in part.

The solar electric industry, however, is one that is filled with a myriad of complicated issues that inhibit the industry from reaching its full potential. To make the industry economically viable there is the need to lower the costs of module production to below $1/watt while at the same time ensuring higher (greater than 15%) module efficiencies [3]. To add to the complexity of the situation, many consumers have limited

real-estate available for solar electric production. This means that, in effect, the solar electric market for non commercial individual consumers is based on available real-estate. With large percentages of the population, especially in cities, living in apartment style high-rise complexes, the available real-estate for individual consumers is highly limited. Hence, the need for very high efficiency devices is even more pronounced.

1.1. Need for Light Trapping in Thin Silicon Solar Cells

To meet all the aforementioned challenges, various avenues of exploration have come to the fore. One technology that has generated considerable interest is thin silicon solar cells (TSSC). By their very nature TSSC reduce the amount of material needed in manufacturing each solar cell and hence ultimately reduce the cost per watt of output power. However, the reduction in active photovoltaic material also compromises the cell efficiency and consequently the need for optimized optical design arises [4], [5]. Light trapping affords the capacity to reduce the thickness of the active solar cell material while still maintaining, in theory, similar absorption characteristics as that of thicker cells. This means that with the addition of an appropriate light trapping scheme the efficiencies of standard commercial cells can be achieved with much less material.

In this thesis we focus our attention on crystalline silicon (c-Si) and all designs presented are based on c-Si as the active photovoltaic material. Crystalline silicon is our chosen material because it has high device efficiency potential, is abundant, is stable and

has well established technologies which are pertinent to the development of nano scale light trapping structures. Throughout this thesis the word silicon is used to refer to c-Si.

1.2. Thesis Overview

In this thesis we consider high efficiency c-Si cells that can function well as both stand alone devices and elements in a multi device stack. In the case of the multi device stack arrangements we design cells that would fit into both the lateral architecture and the independently contacted vertical junction stack that was presented by Barnett et al [6]. In the lateral architecture, incident light is split into spectral components that are then diverted to cells of different band gap energies.

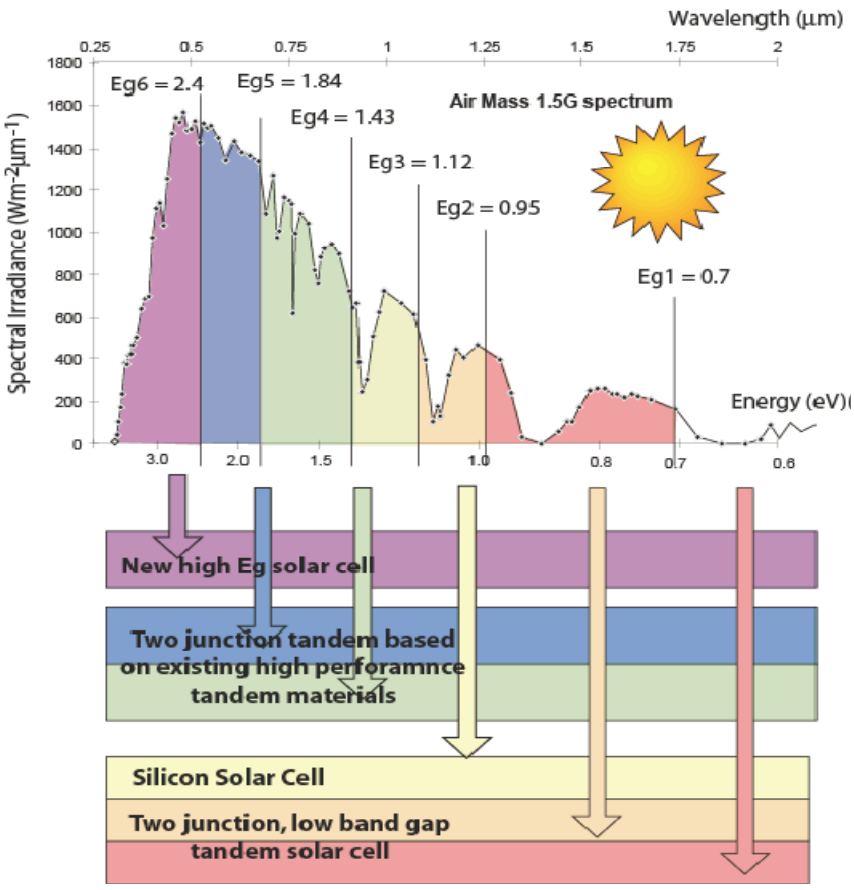

Figure 1.1 Schematic of the stacking architecture for multi-junction solar cell described in [7][6].

In the vertical stack approach, high energy cells are stacked on top of lower band gap cells and hence, only the energy that is unabsorbed by cells higher up in the stack trickles down to the low energy cells, as shown in Fig. 1.1. We design silicon cells that would function well as mid band gap energy cells in both architectures. In the lateral case the light would be split in a way that only bandwidths unabsorbed by higher energy cells would be incident on our mid energy silicon cells. In the vertical junction stack our silicon cell would be placed below a Gallium Arsenide cell (with band gap of 1.43 eV).

For our cells to function well as both single junction and as elements in the aforementioned architectures, we first optimize the light trapping parameters for the 400 – 1100 nm wavelength range. We then consider the enhancement factor in the 867 – 1100 nm range because this would be the band of available incident light on our silicon solar cells when placed in the aforementioned architectures. Finally we analyze the short circuit characteristics of our designs as compared to non modified cells in the full 400 – 1100 nm range to establish their viability as stand alone devices.

Light trapping in solar cells mainly falls into two categories, the first being the reduction of front surface reflection and the second involves increasing the optical path length of light within the cell. In our study, we combine planar anti reflective (AR) coatings with nano structured diffractive gratings to enhance the light trapping capabilities of the solar cells and hence increase the short circuit current characteristics of the device. To model the devices we employ the scattering matrix method [8],[9] and particle swarm optimization algorithm [10],[11].

1.3 List of Original Contributions

This thesis includes most of the original work that we did in the first two phases of the VHESC project. The contributions presented in this thesis are:

1. Optimization of anti reflective coating designs for thin c-Si solar cell applications.
2. Fabrication and characterization of broadband triple layer antireflective coatings that matched well with the optimization results.

3. Design of high light trapping efficiency single junction design structures with Jsc values that came close to the geometric light trapping limit for 5 micron solar cell structures.
4. Design of multi junction design structures that incorporate one dimensional photonic crystals as selective light filters to enhance light trapping in multiple stack device architectures.

The original contributions have been presented in a peer reviewed journal publication and in an oral presentation at a conference.

Peer Reviewed Journal Publication:

1. J. G. Mutitu, S. Shi, C. Chen, T. Creazzo, A. Barnett, C. Honsberg, and D. W. Prather, "Thin film solar cell design based on photonic crystal and diffractive grating structures", Opt. Express **16**, 2008, 15238-15248**.**

Conference Presentation:

1. J. G. Mutitu, S. Shi, C. Chen, T. Creazzo, A. Barnett, C. Honsberg, and D. W. Prather, "Light Trapping Designs for Thin Film Silicon Solar Cells", presented at IGERT: Solar Hydrogen Conference, 2008.

Acknowledgement

This research was, in part, funded by the U.S. Government Defense Advanced Research Projects Agency under Agreement No.: HR0011-0709-0005.

Chapter 2

SOLAR CELL OPERATION AND THIN SILICON SOLAR CELLS

2.1 Solar Cell Operation

This section of this thesis is concerned with articulating the process of power generation in solar cells with some emphasis on the light generated current, which is pertinent to the science of light trapping. A brief discussion is then presented on how the light generated current relates to the overall solar cell efficiency.

A photovoltaic device can be described as a type of direct converter of solar light into electricity. This process occurs when incident photons on a semiconductor device structure are absorbed and thus generate electrical carriers, electrons and holes, which are then collected in order to create electrical power. The physics in the active photovoltaic region is that of a p-n junction, which forms the fundamental operation principles of a vast array of electronic devices, i.e., from LED's to computer microprocessors [12].

2.1.1 Absorption of Light

When light is incident of the surface of a solar cell, it will either be reflected or transmitted into the solar cell material. Of the light that enters the solar cell, some of it will be absorbed and the rest will escape through the various facets of the solar cell structure. The escaping light is due to a number of processes which include, but are not

limited to, transmission, reflection off the back surface and internal scattering. The intensity of light that is transmitted into the solar cell gets attenuated as it passes through the photovoltaic material. This attenuation, or rate of absorption, is proportional to the intensity of the light at a given wavelength. The decay in intensity, of monochromatic light passing through the solar cell, is exponential in nature and can be described mathematically as:

$$I(x) = I_0 e^{-\alpha x} \tag{2.1}$$

where I is the intensity, x is the depth into the material and α is the absorption coefficient.

The absorption coefficient is a wavelength dependent material parameter that determines how far into a material a light wave can penetrate before being absorbed. [13],[12].

Using the equation for the light intensity, Eqn. 2.1, it is possible to calculate the number of electron-hole pairs (e-h pairs) that are being generated within the solar cell. To do this, it must be assumed that the loss in intensity is directly responsible for the generation of an e-h pair. Hence, the generation rate, G, in a thin slice of the solar cell is gotten by calculating the change in light intensity across the slice, i.e., taking a derivative of the intensity. So, the generation rate is given by

$$G(x) = \alpha N_0 e^{-\alpha x} \tag{2.2}$$

where N_0 is the photon flux at the solar cell surface in units of photons/unit-area/sec,α is the absorption coefficient and x is the distance into the solar cell [13],[12].

The light that is absorbed is not of a single wavelength and hence, has various energies associated with the individual wavelengths, i.e., different photon energies. The

variance in photon energy causes various effects, in the active photovoltaic region, which can be summarized into three categories. These three categories are dependent on the energy of the incident photon (Eph) and the bandgap of the semiconductor material (EG) and can be classified as follows [13],[12].

1. If Eph < EG, then the photons interact weakly with the semiconductor and pass right through the active photovoltaic region without being absorbed.

2. If Eph = EG, then the incident photon transfers its energy to an electron, hence moving it up from the valence band to the conduction band, and thus creating an e-h pair.

3. If Eph > EG then the photon is strongly absorbed; it transfers its energy to the electron, and the electron gets excited to an energy level beyond the conduction band. Finally the e-h pair releases the excess energy as thermal energy and they finally relax back to the band edges. The excess energy is wasted.

In an indirect semiconductor, such as c-Si, the minimum energy point on the conduction band and the maximum energy point on the valence band occur at different values of crystal momentum [13],[12].Hence, introducing the need for another fundamental (quantum) particle in order for an electron to transition from valence to conduction band. Due to the fact that an additional particle is involved in the photon absorption - electron excitation process, the absorption coefficient is low and hence, the absorption depth of light increases. The absorption depth is the distance a light wave travels inside the semiconductor before being absorbed; it is the distance which light

travels in a material before dropping to 36% of its original intensity [13],[12]. It is defined as the reciprocal of the absorption coefficient and it explains why c-Si has poor intrinsic absorption near its band edge.

2.1.2 Light Generated Current

If a photon with sufficient energy (≥ EG) is absorbed, an e-h pair is generated. However, electrons that exist on the p-type side and holes on n-type side of the p-n junction are metastable, i.e., they only exist for a minority carrier lifetime, before being lost to recombination. When carriers recombine, no electrical power is generated. To this end, the p-n junction acts to spatially separate the light generated carriers by the process of carrier collection. The electric field due to the p-n junction sweeps the light generated minority carriers across the junction and hence, making them (the carriers), majority carriers. If contacts are then connected to the emitter and base region of the solar cell, the light generated carriers flow in the external circuit [12]. This light generated current flows opposite to the direction of the diode current and thus creates reverse bias operation. This can be seen by looking at the diode equations for a solar cell that is in the dark and one that is illuminated. The ideal diode equation for a solar cell in the dark is given by,

$$I_{Diode} = I_0\left[\exp\left(\frac{q\cdot V}{kT}\right)-1\right] \tag{2.3}$$

and when the solar cell is illuminated the diode current becomes,

$$I_{Diode} = I_0\left[\exp\left(\frac{q \cdot V}{kT}\right) - 1\right] - I_{Light} \tag{2.4}$$

where I_{Diode} is the current flowing through the diode, I_o is the dark saturation current i.e. the diode leakage current with no illumination, V is the applied voltage across the diode, q is the absolute electron charge, k is Boltzmann's constant, T is the absolute temperature and I_{Light} is the light generated current.

The dark saturation current is a measure of the recombination in a diode, i.e., a diode with higher I_o has higher recombination, it can be used to differentiate between diodes [13],[12], [14].

When the solar cell is in the dark, it has the same I-V characteristics as a very large diode. The illumination and consequent generation of I_{Light} has the effect of shifting the I-V curve down into the fourth quadrant and hence, power is generated.

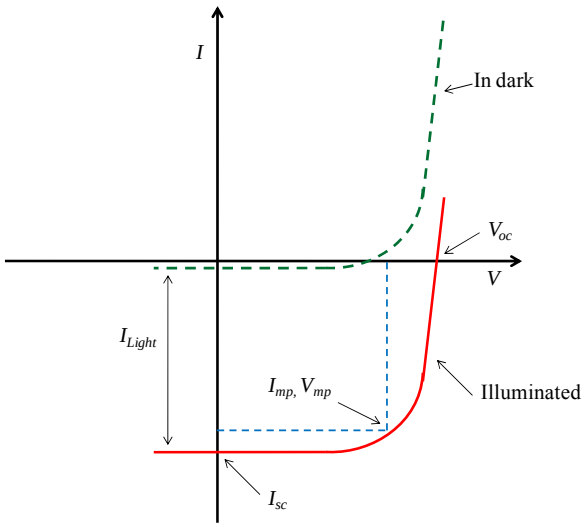

Figure 2.1 Current and voltage characteristics of a solar cell when in the dark and when illuminated.

The I-V curve can be used to determine a number of important parameters that characterize the performance of a solar cell. The first of these is the short circuit current, Isc, as shown in Fig. 2.1.

2.1.3 Short Circuit Current

The short circuit current is the maximum current that can be derived from the solar cell, i.e., when it is short circuited; with no voltage across the solar cell. For ideal solar cells, with no highly resistive losses, less than 10 Ωcm^2, the short circuit current is equal to the light generated current (I_{Light} = Isc). The short circuit current is dependent on a number of factors which are: the area of the solar cell, the power of the incident light, the spectrum of the incident light, the absorption characteristics and the collection probability. The short circuit current, Isc, is usually expressed as a current density, Jsc with units of mA/cm^2 and hence, the calculation for Jsc is not dependent on solar cell area.

The most critical material parameters in comparing the Jsc of solar cells of the same material type are the surface passivation and diffusion length. The carrier diffusion length is defined as the distance in the solar cell that a carrier will move from the point at which it is generated to the point at which it recombines. If we assume a perfectly passivated solar cell with uniform generation rate, the Jsc can be approximated by

$$Jsc = qG(L_n + L_p) \tag{2.5}$$

Where q is the electron charge, G is the generation rate, L_n is the electron diffusion length and L_p is the hole diffusion length [13],[12], [14].

2.1.4 Open Circuit Voltage

Another parameter used to characterize solar cell output is the open circuit voltage Voc. The Voc is the maximum voltage that can be gotten from a solar cell; when the current is zero. The Voc is determined by the properties of the semiconductor. The equation for Voc is given by,

$$V_{oc} = \frac{kT}{q} \ln\left(\frac{I_{Light}}{I_0} + 1 \right) \tag{2.6}$$

where I_o is the dark saturation current, q is the absolute electron charge, k is Boltzmann's constant, T is the absolute temperature, and I_{Light} is the light generated current.

2.1.5 Fill Factor

The third parameter used to characterize solar cell performance is called the fill factor (FF). The FF is defined as the ratio of the maximum power that can be derived from a solar cell to the product of the Jsc and Voc. At the points where the Jsc and Voc occur, no power is generated because the occurrence of one of these parameters means that the other is zero. The FF is therefore the area of the largest rectangle that can fit into the I-V curve and is hence, described as a measure of the squareness of the I-V characteristics of a solar cell under illumination. It can be calculated using,

$$FF = \frac{J_{mp} \times V_{mp}}{J_{sc} \times V_{oc}} \tag{2.7}$$

2.1.6 Solar Cell Efficiency

The final parameter used in characterizing the performance of a solar cell is the efficiency. The efficiency is defined as the ratio of the power that is output by the solar cell, to the power that is incident on the solar cell. The efficiency can be calculated using,

$$Efficiency = \frac{J_{sc} \times V_{oc} \times FF}{P_{in}} \tag{2.8}$$

The efficiency of a solar cell is affected by the intensity and spectrum of incident light as well as the temperature of the solar cell. Efficiency measurements are standardized to a temperature of 25 degrees and AM1.5G illumination spectrum. The AM1.5G illumination is the standard irradiance spectrum at the earth's surface; it accounts for losses in solar intensity and power as the light passes through the atmosphere and gets absorbed by air and dust. The G in AM1.5G stands for global and it means that the spectrum includes direct and diffuse solar radiation.

The full range of the intricate science of semiconductor device physics, especially as it applies to solar cells, is vast and well articulated in many texts such as [13],[12], [14].

2.2 Thin Silicon Solar Cells

Thin film solar cells are by definition devices with a thickness of less than 50 microns [4], which is significantly smaller than commercially used silicon wafers with thicknesses of about 100 – 300 microns. In this thesis we will mainly focus on single crystalline

silicon (c-Si) which is the most commonly used material in standard solar cell technology. Crystalline silicon technology is mature and also benefits from having well established material processing methods carried over from the integrated circuit industry. Our work is focused mainly on ultra thin (5 micron) c-Si structures. The greatest advantage that thin silicon solar cells present is that the amount of material needed in manufacturing each solar cell is significantly reduced, as shown in Fig 2.2. The second advantage is that the reduction in cell thickness improves the collection efficiency of e-h pairs, especially in c-Si structures. If photons are not absorbed within a diffusion length of the junction then the light generated carriers are lost to recombination [13],[12], [14]. It is important to note here that an effective way of minimizing recombination losses in a silicon solar cell, including bulk recombination, thus maximizing open circuit voltage, is by reducing the volume of the cell [13],[12], [14].

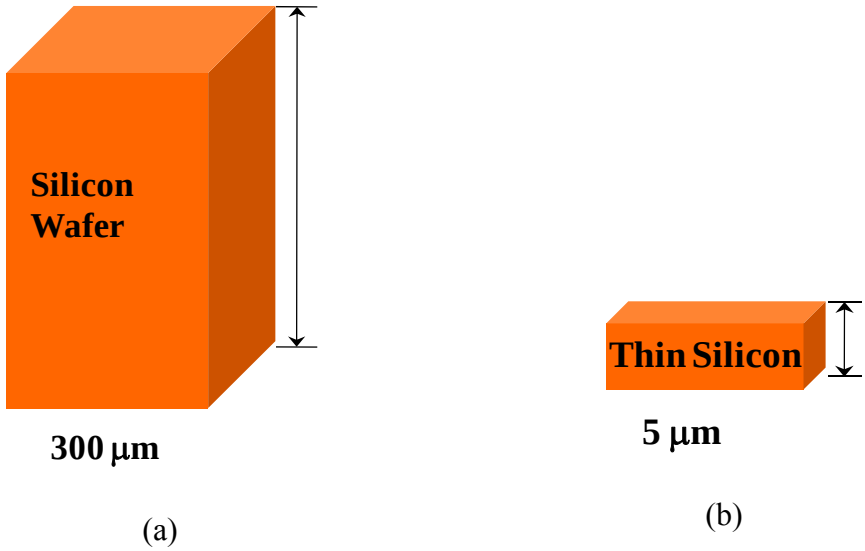

Figure 2.2 (a) Diagrammatic representation of conventional silicon solar cell of 300 micron thickness, (b) thin silicon, 5 micron, structure.

The third advantage is that thin film technology offers prospects for reducing material losses, especially the apparent losses of high quality silicon as sawdust from CZ grown ingots. To this end, many thin film deposition techniques are being investigated [15], [16], which will ultimately reduce the overall costs by eliminating the cost of silicon wafers. Finally, thin film technology has the added advantage of increasing the size of the unit of manufacturing, i.e., the unit size is not constrained to the area of a silicon wafer [17].

However thin c-Si also has a number of disadvantages brought about by the physical stature of the device region. At short wavelengths of light, c-Si is strongly absorbing as can be affirmed by the high values of its absorption coefficient at shorter (UV- Visible) wavelengths. Due to its indirect band gap, c-Si is weakly absorbing in the near infrared regime of the solar spectrum which can be attested by the increase in absorption length (reciprocal of absorption coefficient) from 11 microns at 800 nm to over 3 mm at 1100 nm [18]. This effect makes it difficult to achieve high performance thin film devices with thicknesses in the order of a few microns. Therefore, the ideal goal is to get a thinner cell which maintains the effective optical thickness of a thicker cell. Consequently, there is a need for light trapping architectures that increase the optical path length of light within the solar cell and thereby increase the overall cell efficiency. The topic of light trapping in thin silicon solar cells is introduced in the next chapter.

Chapter 3

INTRODUCTION TO LIGHT TRAPPING

To increase the efficiency of terrestrial solar cells one has to consider the fact that the study of solar cells is a multidisciplinary science that encompasses many branches of physics and engineering. One very important branch of solar cell design is optics, which includes the lenses used for concentrating incident light, reducing the reflection from the front surface and increasing the optical path length of light within the solar cell. So, we can describe light trapping as the branch of the optics of solar cells that involves capturing and keeping the most amount of light within the solar cell structure for the longest time.

One may then ask why it would be beneficial to retain the light within a solar cell for a longer time. The answer to this question is that, the longer a photon stays within a solar cell the greater the chances it has of being absorbed and creating an e-h pair and hence increasing the short circuit current characteristics of the solar cell. Another important advantage light trapping affords, is the capacity to reduce the thickness of the solar cell while still maintaining, in theory, similar absorption characteristics as thicker cells. It is important to note here that an effective way of minimizing recombination losses in a solar cell, including bulk recombination, thus maximizing open circuit voltage, is by reducing the volume of the cell [18]. This would be achieved best by reducing the

thickness of the solar cell, because the top surface area is essential in the capture of incoming light. The science of effectively reducing the cell thickness, however, is not a trivial one. Many tradeoffs arise in the optimization of cell open circuit voltage because of the very nature of the parameters influencing the diffusion length, i.e., diffusion length is influenced by the processing of the wafer, the material type and the doping of the wafer. Also, in terms of cell thickness, if photons are not absorbed within a diffusion length of the junction then the light generated carriers are lost to recombination. So it is ideal to get a thinner cell which maintains the effective optical thickness of a thicker cell [18],[17],[12].

3.1 Objectives of Light Trapping

Light trapping is concerned with increasing the short circuit current characteristics of the solar cell device structure. This is achieved through increasing the absorption characteristics which are related to the short circuit current by the following equation

$$J_{sc} = \frac{q}{hc} \int_{\lambda} \lambda' A(\lambda') Irrd(\lambda') d\lambda' \tag{3.1}$$

where J_{sc} is the short circuit current density, q is the charge on an electron, h is Planck's constant, c is the speed of light, λ is the wavelength, A is the absorption of the silicon structure and $Irrd$ is the solar irradiance spectrum [4]. As you may recall, the Jsc is related to the efficiency by Eqn. 2.7 (from chapter 2),

$$Efficiency = \frac{J_{sc} \times V_{oc} \times FF}{P_{in}}$$

Hence, an increase in Jsc directly influences the efficiency of a solar cell device. It is therefore, pertinent to maximize the short circuit current if one wishes to achieve very high efficiency solar cells. In this respect, we use the Jsc as our figure of merit when optimizing design parameters of the solar cell design architecture. It is worthy to note, that the figure of merit is an optimization parameter, rather than a photovoltaic device affiliated parameter.

3.2 Limits of Light Trapping

With a clearly identified objective, the next course of action involves the identification of the limits of the study. The limits enable us to understand what we are shooting for and hence give us a metric for the performance of the final design and device structures. In this study, as is with all studies that concern silicon, the wavelength range of interest is 400nm – 1100 nm. If we take the absorption to be unity and apply the Jsc equation, Eqn. 3.1, in the 400 – 1100 nm wavelength range, the resultant Jsc is 43.12 mA/cm^2. This value represents the maximum Jsc achievable over this wavelength range under the illumination of 1 sun. The second limit worth identifying is the Jsc limit of a 5 micron device structure, with no light trapping structures, but incorporated in bulk material. This means that the incident light is propagating through silicon, and enters the silicon structure, thereby including no reflection losses at the front surface, as shown in Fig. 3.1.

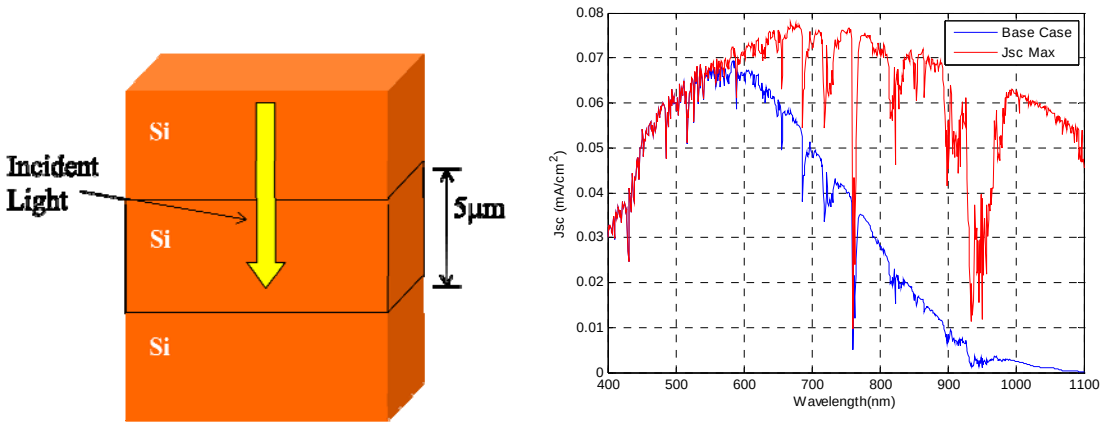

(a) (b)

Figure 3.1 Depiction of light wave travelling through bulk silicon and incident on a 5 micron segment (b) graph of Jsc characteristics for the maximum available Jsc (red graph) and amount generated in the 5 micron structure from (a). The Jsc value for this structure is 23.4 mA/cm^2.

The wave then propagates through the solar cell structure where some of the power gets absorbed and then finally transmits through the silicon region of interest and into bulk silicon; without any back surface reflectance. The Jsc value for this 5 micron device structure is 23.4 mA/cm^2.

The next limit of interest is the geometric light trapping limit, which involves the optical path length of light within a solar cell structure. The optical path length is described as the path a photon takes within a solar cell and its distance is measured in terms of the thickness of the solar cell. For example, a cell without any light trapping will have the incident wave pass through the solar cell once and transmit through the base of the cell. So in terms of optical path length, we say that it has a value of one. If we

introduced a reflector at the base of the solar cell, which normally reflects the incident waves, then we can say that the optical path length, or effective cell thickness, is two.

The maximum optical path length enhancement, using geometric optical light trapping, was derived using a statistical mechanics approach towards the optics of textured and inhomogeneous optical sheets by Yablonovitch and Cody [19]. It was found to be a factor of $4n^2$, where n is the refractive index of the material; it works out to be 50 for silicon, assuming a uniform refractive index of 3.5. Using this light trapping limit, the equation for the maximum absorption becomes,

$$A(\lambda) = 1 - \exp(-\alpha_s(\lambda) 4 n_s^2(\lambda)\ W_{eff}) \tag{3.2}$$

where α is the absorption coefficient of silicon, n_s is the refractive index of silicon and W_{eff} is effective thickness of the device structure.

The Jsc limit for a 5 micron structure, derived using Eqn. 3.3, is 39.7 mA/cm^2. All the aforementioned limits are summarized in table 3.1.

Table 3.1 Short circuit current limits for a 5 micron device structure and the maximum available value

Device Structure	Jsc (mA/cm^2)
Limit (i.e., Absorption = 100%)	**43.12**
Plain silicon slab with no light trapping 5 microns thick	**23.4**
Limit for 5 micron device (optimal)	**39.7**

3.3 Geometric and Wave Optical Light Trapping

There has been much work done on light trapping based on principles of geometric optics [4] with the upper limit (of $4n^2$)[19] attained by the incorporation of Lambertian light trapping schemes, i.e., schemes that scatter reflected and transmitted light with uniform brightness in all directions [4],[18]. However, the geometrical light trapping limit holds mainly for cells with an isotropic response (a cell that gives the same response regardless of incident angle) and is not optimal for normally incident illumination.

In recent years it has been shown that the geometric light trapping limit in indirect bandgap semiconductors such as c-Si, that was derived by Yablonovitch and Cody [19] to be a factor of $4n^2$ **(**where n is the refractive index of the solar cell material), can be surpassed using a wave optics approach. In chapter two of the book 'Thin-Film Crystalline Silicon Solar Cells' by Rolf Brendel, a theoretical proof of this idea, utilizing a gedanken experiment, is presented [4]. With the advent of powerful computational tools and sub micron material processing techniques it is now possible to design effective light trapping schemes utilizing the wave nature of light. In this thesis we utilize a wave optics approach and use electromagnetic tools we developed to optimize and model solar cell structures that include sub micron features.

We have also, using the wave optics approach, been able to model multi device stack arrangements [20]. In these particular arrangements, cells with different bandgaps are stacked, in order of increasing wavelength absorption, to fully utilize the solar

spectrum. We have designed silicon solar cells that fit into multi device architectures and utilized a one dimensional photonic crystal (1D-PhC) to act as a selective light filter at the interface between two cells. The incorporation of the 1D-PhC also allows for unabsorbed wavelengths to propagate to underlying lower energy cells further down in the stack.

3.4 Enhancement Factor

If we take a look at the graphs for the absorption and transmission of the structure in Fig. 3.1(a), (graphs in Fig. 3.2) it is evident that c-Si is a poor absorber of wavelengths close to the silicon band gap i.e. 1108 nm. If we observe the absorption characteristics, as shown in Fig. 3.2(a), we immediately see that from about 550 nm, c-Si starts to decrease in its absorption capability. By the time we get out to 900 nm, the loss is almost total.

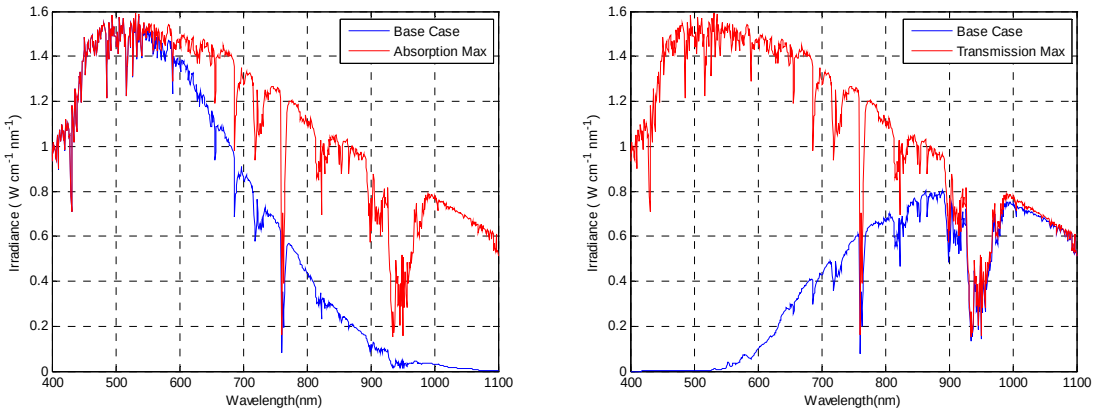

(a) (b)

Figure 3.2 (a) Graph of absorbed power (blue plot) as compared to the power available from the sun (red plot), (b) graph of transmission characteristics (blue plot) of 5 micron solar cell structure.

It is necessary to quantify what is at stake in this small region of the solar spectrum. We first define the region of interest, i.e., the silicon band edge as the 867 – 1100 nm range. We choose this wavelength range because it corresponds to the light available after being split or passed down from a GaAs cell (with a band gap of 1.43 eV). This choice assumes that the silicon cell is part of the multi device architecture described by Barnett et al [6], and hence, all the wavelengths below 867 nm are absorbed by other, higher energy cells. It is also worthy to note that in this wavelength range, c-Si due to its indirect band gap, has poor intrinsic absorption; particularly in thin film solar cells.

In this wavelength region, i.e., 867 – 1100 nm, c-Si only absorbs 7.8% of the incident irradiance; which works out to be 1.64% of the total irradiance in the 400 – 1100 nm wavelength region. Hence, the need for light trapping in this specific region is self evident.

To measure the performance of our light trapping structures, we define a new quantity for band edge enhancement; the enhancement factor (EF). The EF is the ratio of the average absorption of a modified silicon solar cell to the average absorption of a silicon cell with no light trapping structures. It is important to note that use of the term band edge enhancement factor is a bit of a misnomer because the term was actually used to show the enhancement in a silicon cell placed in the multiple device stack architectures described in [6], i.e. below a Gallium Arsenide cell (with a band gap of 1.43 eV). We continue with the use of this term for purposes of consistency, continuity and comparison with the designs that we worked on, originally. We calculate the absorption of an

enhanced structure for a given spectrum range near the silicon band edge (in this case 867 - 1100 nm) and normalize it to the absorption characteristics of a cell without any light trapping structures as shown in Eqn. 3.4.

$$EF(\lambda) = \frac{\int_{\lambda}^{\lambda=1100} A_E(\lambda')Irrd(\lambda')d\lambda'}{\int_{\lambda}^{\lambda=1100} A_s(\lambda')Irrd(\lambda')d\lambda'} \tag{3.3}$$

where the value A_E represents the absorption characteristics of an enhanced structure, i.e. , with the AR coating at the top surface and light trapping structures at the bottom surface, A_S represents the absorption of a silicon structure with no light trapping structures at the top or bottom surfaces.

When calculating the enhancement factor, we take 1100 nm as the upper limit of integration and for the lower limit we specify a wavelength whose interval with the upper limit defines the domain of integration which specifies the enhancement region and hence the EF is a function of the wavelength.

Chapter 4

LIGHT TRAPPING OPTICS

This chapter is concerned with explaining the concept of light trapping as it applies to c-Si solar cells. The path that a light wave takes as it passes from free space, to the point that the photon energy is absorbed into the active photovoltaic region, is a subject that demands a lot of attention. As light propagates through a vacuum, with a dielectric constant of 1, there is hardly any attenuation or reflection. However when it encounters a medium with a different refractive index, nature dictates that the light will get reflected, transmitted or absorbed by the material medium. These three phenomena are in essence the fundamental principles that govern the science of light trapping. Hence, it is worthwhile to take a closer look at how the science of light trapping is employed to a silicon solar cell and observe the benefits associated with the addition of each optical structure.

4.1 Bare Silicon

We begin with a light wave that propagates through free space and is normally incident on the surface of bare silicon (c-Si), i.e., silicon with no antireflective coating, as shown in Fig. 4.1. It is important to note that throughout this thesis the term silicon is used to refer to c-Si, unless indicated otherwise. The first thing we observe is that a significant

portion of the light is lost to reflection. We can further understand this occurrence by looking at some of the physics associated with the front surface reflectance. Crystalline silicon, for example, has a refractive index of 3.6 at 900 nm and air has refractive index of 1. We can hence calculate the reflection coefficient of the bare silicon surface using Fresnel's equation

$$\Gamma_{12} = \frac{n_1 - n_2}{n_1 + n_2} = \frac{\eta_2 - \eta_1}{\eta_2 + \eta_1} \tag{4.1}$$

where Γ_{12} is the reflection coefficient, n_1 is the refractive index of the first (incident) medium , n_2 is the index of the second medium, η_1 is the intrinsic impedance of the first medium and η_2 is the impedance of the second medium.

The reflection coefficient is described as the ratio of the amplitudes of the reflected and incident electric fields. The reflectance, i.e., the ratio of the reflected to the incident power densities, is the square of the magnitude of the reflection coefficient [21]. Mathematically the reflectance of c-Si can be expressed as a percentage by multiplying the square of the magnitude of the reflection coefficient, as shown in Eqn. 4.2.

$$\left|\Gamma_{12}\right|^2 \times 100 \tag{4.2}$$

For c-Si, the amount of light that is reflected at λ = 900 nm is 32.18%. This means that 32.18% of the incident energy is lost to front surface reflection, and thus the need to find a way to minimize these reflection losses. A calculation for the total reflectance over the 400 – 1100 nm range is performed using scattering matrix calculations and the value over this range is found to be 35%.

Of the light that is incident on the solar cell, only 40% gets absorbed within the first pass of light through the active photovoltaic region; 25% is transmitted. If every photon in the 40% of light absorbed is converted into an electron-hole pair, with no recombination, a Jsc of 15 mA/cm^2 is achieved. Plots of the respective reflection, absorption and transmission characteristics are presented in Fig. 4.2. This case can be viewed as the non light trapping case; we can consider this as a basis for the effects of light trapping for purposes of illustrating the effects of adding the various optical components.

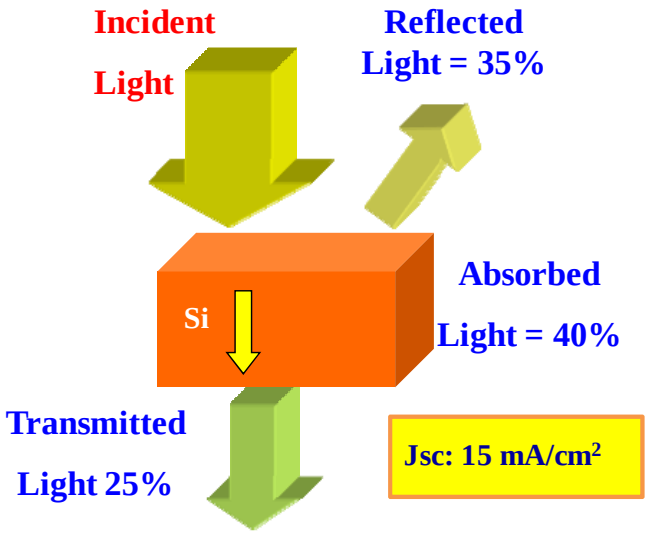

Figure 4.1 Schematic of a plane light wave incident on the surface of bare silicon, 35% of the incident light is reflected, 40% is absorbed and 25% is transmitted. The Jsc of this structure is 15 mA/cm^2.

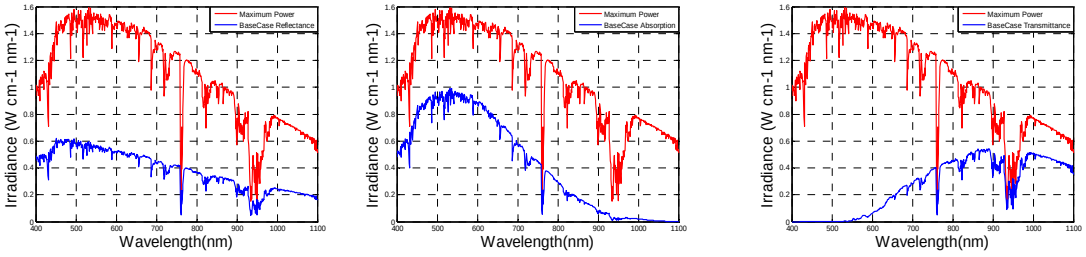

(a) (b) (c)

Figure 4.2 (a) Plot of the amount of light reflected (blue plot) when compared to the total light incident (red plot) on the bare silicon solar cell, (b) similar plot illustrating the absorption characteristics, (c) similar plot illustrating the transmitted irradiance relative to the total incident irradiance.

4.2 Anti-Reflection Coatings

Before we get deeper into the subject of trapping light within the solar cell, we first must address an area of much interest in light trapping optics, i.e., getting the maximum amount of incident light into the cell. In other words, the aforementioned area is concerned with reducing front surface reflection or increasing front surface anti-reflection. In the continuation of our discussion on reducing optical losses from a bare silicon slab, we introduce an anti-reflective coating (AR coating). An AR coating is nothing more than layers of mainly dielectric material that are applied to a surface to reduce the reflectance. The concept of reducing the surface reflectivity by introducing intermediate transparent layers has been known since the early 1800's [22]. These intermediate layers serve to 'buffer' the drastic refractive index changes between low index and higher index materials. So, in our case, one needs to find materials with refractive indices in between those of air and silicon in order to ease the transition of light

from the low to high index material. To this end, antireflective schemes have become necessary in the design and fabrication of solar cells.

To further enhance our understanding how an AR coating works, we consider a brief mathematical treatment. We consider a situation where we have three media, the first being free space, the second, the AR coating material and the third is c-Si. Reverting back to Fresnel's equation, but in this case considering an AR coating sandwiched between two semi infinite materials, the input reflection coefficient, Γ_{in}, can be approximated as:

$$\Gamma_{in} = \Gamma_{12} + \Gamma_{23} e^{-j2\beta_2 t} \tag{4.3}$$

where Γ_{12} is the reflection coefficient of the interface between the first and second medium (free space and AR coating), similarly Γ_{23} is the reflection coefficient between the second and third medium (AR coating and c-Si), β_2 is the phase constant and t is the thickness of the AR coating material.

So, in the case of a good AR coating, it would be desirable to have the input reflection coefficient equal to zero. For this to occur, we set the thickness of the AR coating as a quarter of the wavelength of the input wave in the dielectric material; this concept is the same as that of the quarter wavelength transformer from transmission line theory. So, we want to get the input reflection coefficient as zero, as shown in Eqn. 4.4.

$$\left|\Gamma_{in}\right| = \left|\Gamma_{12} + \Gamma_{23} e^{-j2\beta_2 t}\right| = 0 \tag{4.4}$$

Hence, we set $t = \lambda_2/4$, where $\lambda_2 = \lambda_0/n_2$, i.e., the index of the wave in material 2 (inside the AR coating). From Eqn. 4.4, we can see that,

$$2\beta_2 t = 2\left(\frac{2\pi}{\lambda_2}\right)\left(\frac{\lambda_2}{4}\right) = \pi \tag{4.5}$$

By substituting π into the equation for Γ_{in}, that has been set to zero, the expression for the reflection coefficient works out to [21].

$$2\left|\eta_2^2 + \eta_1\eta_3\right| = 0 \tag{4.6}$$

which implies that,

$$\eta_2 = \sqrt{\eta_1\eta_3} \Rightarrow n_2 = \sqrt{n_1 n_3} \tag{4.7}$$

where n_2 is the refractive index of the AR coating, n_1 is the index of free space and n_3 is the index of the c-Si solar cell material. So for the silicon air interface, with an incident wave with a wavelength of 900 nm and with n_1 = 1 and n_3 = 3.6; n2 should be equal to 1.9, and t = 900/ (4*1.9) = 118 nm.

The presented analysis shows that an AR coating causes a π phase change between the incident and reflected waves, off the surface of the solar cell, and hence causes the two waves to destructively interfere. The destructive interference results in no reflected power and hence, surface antireflection is achieved. An excellent and comprehensive treatment of the AR coating equations and theory can be found in chapter 5 of [21].

In practice, combinations of materials, such as silicon dioxide (SiO_2), titanium dioxide (TiO_2), silicon nitride (Si_3N_4) and some transparent conductive oxides are commonly used as AR coating materials for c-Si [23],[24].

4.3 Silicon with AR Coating

The second case we consider is one where an antireflection coating has been added to the bare silicon structure of Fig. 4.1. In this case, for reasons of simplicity, the refractive index is set as the geometric mean of the index of free space and that of silicon at λ_0 = 900nm, and the thickness is set to be $\lambda_0/4n_2$. With such an AR coating applied, the front surface reflectance is now reduced to 8% of the total incident power. Similarly the amount of light absorbed increases, for there is more light that actually enters the active photovoltaic region than in the previous case. The absorbed light is now 57%, which is 17% more than was absorbed for the bare silicon case. Again, as was anticipated, there is now more light to transmit, and hence, the transmission increases by 10% to a value of 35%, i.e., when compared to the bare silicon case; as shown in Fig. 4.3. It is interesting to see just how drastically all the values change when compared to the initial case, and the characteristic graphs of the two cases are plotted and compared to the total incident flux in Fig. 4.4. The green graphs in Fig. 4.4 represent the characteristics of the enhanced (with AR coating) structure. The AR coating allows for 27% more of the incident power to propagate through the solar cell structure. Of this amount of light, 17% is absorbed by the active photovoltaic region and 10% is transmitted out of the cell. So, the next logical step in this train of thought is to minimize the transmission losses.

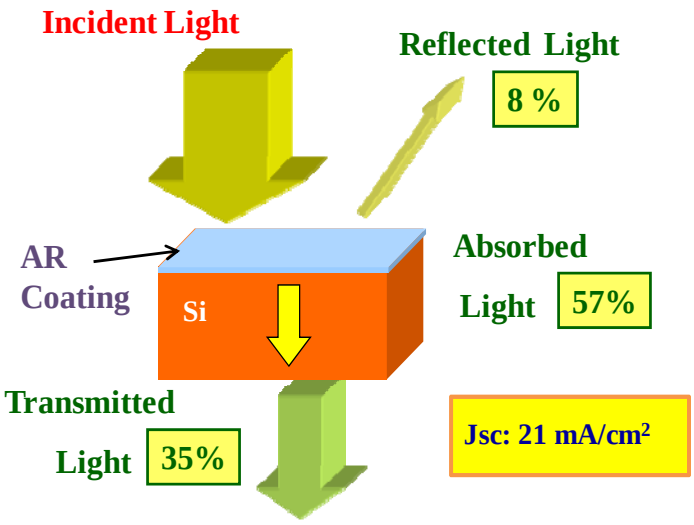

Figure 4.3 Schematic of a plane light wave incident on the surface of silicon with an added AR coating, only 8% of the incident light is now reflected, 57% is absorbed and 35% is transmitted. The Jsc of this structure is 21 mA/cm^2.

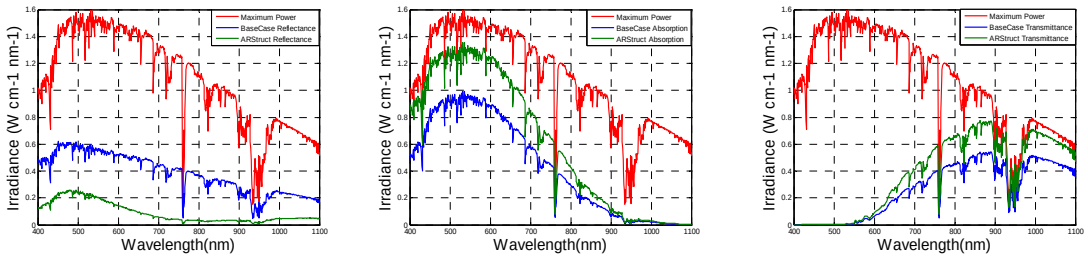

(a) (b) (c)

Figure 4.4 (a) Plot of the amount of light reflected by the structure of Fig 4.3 (green plot) when compared to the total light incident (red plot) and the reflectance of the bare silicon solar cell (blue plot), (b) similar plot illustrating the absorption characteristics, (c) the transmitted irradiance compared to the incident and bare silicon transmitted irradiance.

To effectively design an AR coating one has to realize that the refractive index of materials varies for different wavelengths over the whole solar spectrum and so, one has

to enlist the use of computer software to optimize the thicknesses of the layers of the coating. Also, multiple layers of materials of increasing refractive index are desirable in that they gently increase the index variation from air.

4.4 Silicon Band Edge

At this point it is worthwhile to take a deeper look at the occurrences closer to the silicon band edge. As has been mentioned before, silicon, due its indirect bandgap has poor intrinsic absorption for wavelengths close to the band edge. In this study we consider the 850 – 1100 nm region as being close to the band edge and we first of all see that this region contains 23% of the incident power. However, only 8.7% of the incident power in this region is captured within the first pass of light through the solar cell (this is only 2% of the power in the 400 – 1100 nm region). Figure 4.5 (a) shows the absorption characteristics of the two design structures that have been so far presented; (b) shows how much of the incident light actually gets transmitted. These two graphs properly illustrate the need for light trapping in thin silicon structures and in a sense form the basis from which the rest of the analysis proceeds.

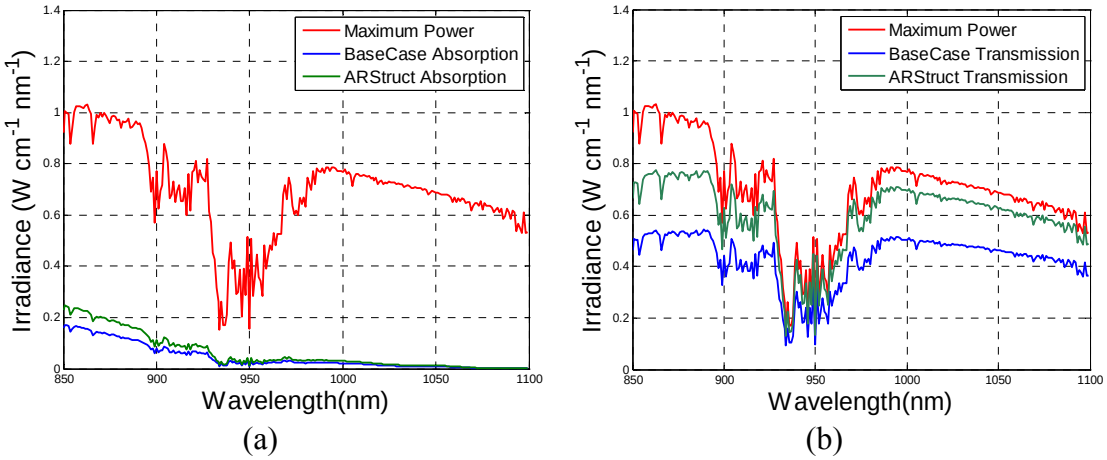

Figure 4.5 (a) Absorption characteristics of the two solar cell structures presented so far. The green plot shows the characteristics of the design structure with an AR coating, the blue plot shows the characteristics of the bare silicon structure and the red plot shows the incident irradiance on the solar cell structures, (b) transmission characteristics of the two structures, compared with the incident power; the color coding is the same as in part (a).

4.5 Silicon with AR Coating and Back Reflector

As had been hinted before, there is the need to reduce the transmittance from the active photovoltaic region. The simplest and most intuitive way of doing this is by the addition of a back surface reflector. This reflector, by its very nature, begins to serve a multiplicity of purposes. We first observe that, with the addition of an idealized back reflector, no light is transmitted. Second, the light that would otherwise be lost is now reflected back into the active region where it can be reabsorbed as it passes through, as shown in Fig. 4.6. With this addition, we have now doubled the optical path length of light through the solar cell. As one can imagine, the total absorption increases; by 10%. One may wonder why the absorption does not double as the path length doubles. This is because many of the shorter wavelengths are absorbed within the first pass of light through the solar cell.

Hence, with the increased path length, we are essentially increasing the effective thickness of the active region, and thus allowing for more photons, with longer absorption depths, to be absorbed.

Another interesting observation is that the reflectance has increased significantly from that of the case with the AR coating only. This happens because of the light that is reflected from the back surface and not yet absorbed within the active silicon region. This light, that would otherwise have been transmitted, now contributes to the overall reflective losses from the solar cell structure. Figure 4.7, shows, in greater detail the effect of the back reflector on the reflectance and absorption characteristics of the solar cell structure. As before, the green plot represents the new structure, i.e., with AR coating and back reflector, the blue plot is that of the bare silicon structure and the red plot represents the incident irradiance.

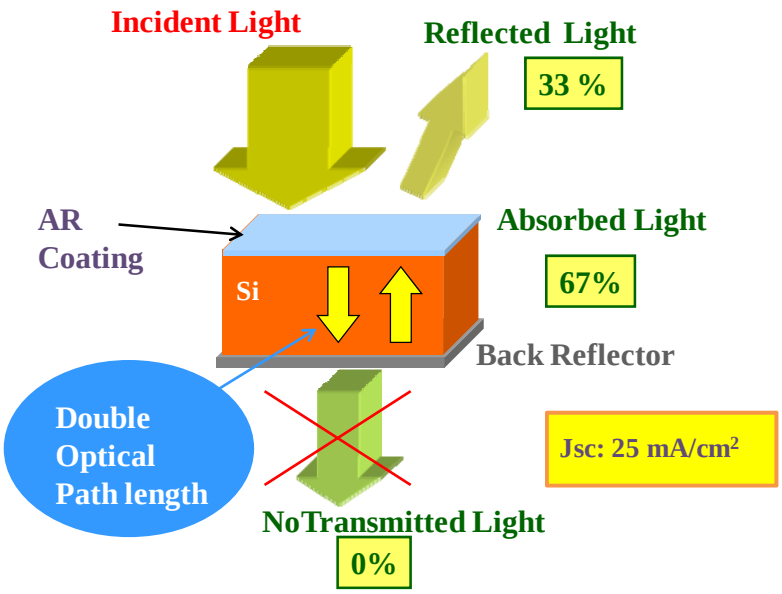

Figure 4.6 Schematic of a plane light wave incident on the surface of silicon with an added AR coating and back reflector, this time 33% of the light is reflected due to light that is reflected from the back surface. The optical path length of light is doubled in this case and the absorption is now 67%. There is no transmitted light. The Jsc of this structure is 25 mA/cm^2

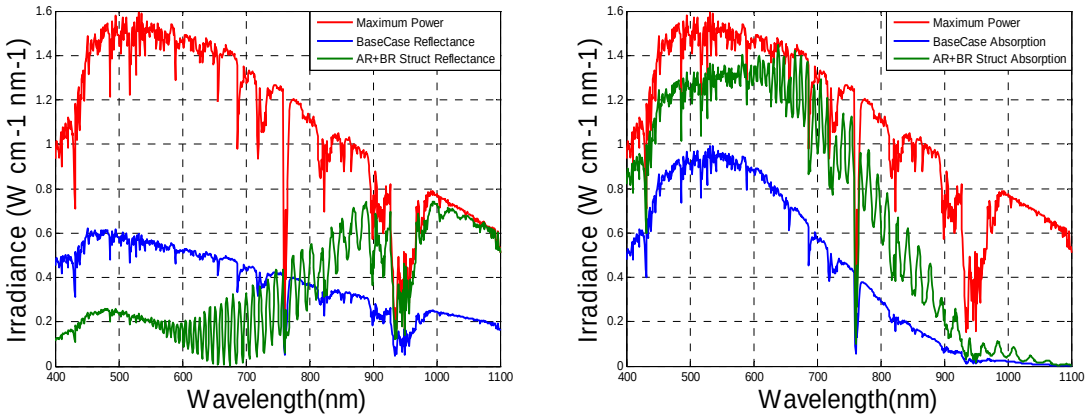

(a) (b)

Figure 4.7 (a) Plot showing the increased reflectance characteristics of the structure with a back reflector. In the figure legends, AR+BR Struct, corresponds to the structure of Fig. 4.6, (b) shows the absorption characteristics, when compared with the incident power and bare silicon structure characteristics.

The addition of the back reflector still does not do much for the light at the silicon band edge. We observe only minor increments of light absorption at those wavelengths and hence, this situation necessitates the addition of a more complex geometry. To this end, we incorporate a diffraction grating, to the back reflector.

4.6 Diffraction Gratings

An interesting historical note on the discovery of the diffraction grating phenomenon is that it was first observed by Francis Hopkinson, who was George Washington's first secretary of the Navy and one of the signers of the American Declaration of Independence [25]. One night in 1785, Hopkinson observed a street lamp at a distance through a fine silk handkerchief and noticed that it produced multiple images which did not change as he changed the position of the handkerchief. He told his friend David Rittenhouse, an astronomer, of his findings and it was Rittnhouse who was able to classify phenomena as being that of diffraction. Later on, Thomas Young independently observed the diffraction effect and was able to distinguish different colors by their wavelengths. The first serious formal treatment on diffraction gratings was undertaken by Joseph von Fraunhoffer, after which most considered him the father of the subject.

The premise of the diffraction grating is that, when a light wave encounters a groove or slit with a period similar to the wavelength of the light, diffraction of the light occurs. A diffraction grating is a periodic arrangement of such grooves or slits. Each groove or slit behaves like a source of light, i.e., for the reflected or transmitted light. The diffracted light waves constructively interfere at specific angles, relative to the grating

normal, which are determined by the geometric proportions of the grating. The phenomena of diffraction gratings can be described with the aid of a simple diagram, as in Fig. 4.8, and a brief mathematical treatment [25],[26].

In Fig. 4.8, a plane wave front is incident on a grating, at an angle θ_{in} relative to the grating normal [25]. There exists a path difference between the light incident on neighboring grooves, and this distance is equal to $d \sin \theta_{in}$; where d is the period of the grating. On reflection from the grating, the path difference is now equal to $d \sin \theta_{out}$; where θ_{out} is equal to the angle of diffraction relative to the normal to the grating. Hence, the total geometric path difference of the light diffracted by the grating is equal to $d \sin \theta_{in} - d \sin \theta_{out}$. For the diffracted light waves to constructively interfere (for the light to be in phase), the path difference must be equal to the wavelength of light or an integral multiple of the wavelength. Hence, giving rise to the famous diffraction grating equation; shown in Eqn. 4.5.

$$m\lambda = d\,(\sin \theta_{out} + \sin \theta_{out}), \quad m = 0, \pm 1, \pm 2, \ldots, \tag{4.5}$$

where m is the integral multiplier.

The integral multiplier, m, denotes the different diffraction orders; when $m = 0$ we have specula reflection. When the light wave is normally incident on the grating, i.e., when $\theta_{in} = 0$, the diffraction grating equation becomes

$$m\lambda = d \sin \theta_{out} \tag{4.6}$$

Diffraction gratings are characterized by three structural parameters, which are: the grating period *d*, the grating depth *H*, and the duty cycle *f*, which is described as the ratio between the groove width and the period.

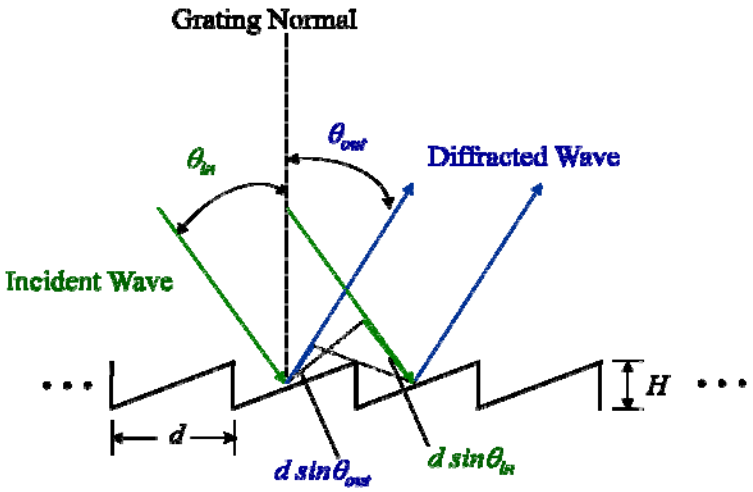

Figure 4.8 Showing a light wave incident and diffracted from a reflective diffraction grating. The geometric path difference between the incident and diffracted wave forms the premise for the diffraction grating equation.

To apply a diffraction grating to a silicon solar cell structure, to increase the optical path length of light within the solar cell, one has to take into account some additional physical processes. The main idea, behind integrating a diffraction grating is to not only increase the path length of diffracted waves, but also to ensure that the waves remain in the silicon structure by means of total internal reflection (TIR). Total internal reflection occurs when a light wave travelling in a high index material, is obliquely incident on an interface between the high index and another lower index material. If the light wave is incident at or beyond a critical angle, it gets totally reflected back into the

higher index medium. This TIR phenomenon follows from Sell's law of refraction, in the case where the angle of refraction is 90 degrees; since the argument of the sine function cannot exceed unity. It is worthy to note that this condition only holds for materials with identical permeabilities, which is true for most dielectrics [21]. The equation for the critical angle is,

$$\theta_c = \sin^{-1}\left(\frac{n_2}{n_1}\right) \tag{4.7}$$

where $n_1 > n_2$.

At 900 nm, the critical angle for c-Si (with a refractive index of 3.6), with free space as the exit medium, is 16.13 degrees. If we include the AR coating, with an index of 1.9, we get the critical angle being $\sin^{-1}(1.9/3.6) = 31.86$ degrees.

We can now modify the diffraction grating equation, by incorporating the critical angle, and hence determine the period of the grating, as shown in Eqn 4.8.

$$d = \frac{m\lambda_0}{n_s \sin\theta_c} \tag{4.8}$$

where λ_0 is the wavelength of light propagating through free space, and n_s is the refractive index of c-Si.

We can now calculate the grating parameters, i.e., when $\lambda_0 = 900$ nm and $n_s = 3.6$; for the first diffraction order, i.e., m = 1, the period $d = 474$ nm.

We now take a step further, since we want the diffraction angle to be greater than the critical angle, and adjust our parameters accordingly. We revert back to the original grating equation, assuming normal incidence, and work out what period we would need

to get close to 90 degree diffraction. We can assume 89 degrees as the angle of diffraction and hence find that the period using

$$d = \frac{m\lambda_0}{n_s \sin\theta_{out}} \tag{4.9}$$

We get, that for the first order, the period would be 294 nm, and for the second order d = 588 nm. At an incident wavelength of 1100 nm, the period for the first order is 359 nm, and d = 718 nm for the second order.

In practice, however, with varied grating materials, varying geometries and dispersion qualities of all the materials involved in the solar cell, it is difficult to find a simplistic analytical solution for the grating parameters. Hence, we use a numerical simulation tool, S-Matrix, to solve Maxwell's equations and then use an optimization algorithm, particle swarm optimization, to achieve the optimal design parameters.

At this juncture, it is worthy to make a number of observations about the grating parameters. First off, in terms of fabrication, the gratings optimized for first order diffraction are more complex to realize. Second, the smaller gratings are also more sensitive to variations in the aspect ratio of the grating and hence have very small fabrication tolerances (within 5%) [26].

4.7 Silicon with AR Coating, Back Reflector and Diffraction Grating

With the addition of the grating, the optical path length is now greatly increased. The light that propagates to the back surface is diffracted into the different orders, with angles greater than the critical angle of silicon. Hence, total internal reflection occurs and the

light is then reflected back to the grating where it is again diffracted, and so on and so forth, as shown in Fig. 4.9. One dimensional (linear) gratings are considered in this study because they are easier to fabricate and also they can be used to trap light of both polarizations.

In the case of the structure with the added diffraction grating, the absorption increases by a further 17% from the structure with a back reflector and AR coating only. It is worthy to note that the total absorption is more than double that of a structure with no added light trapping. The Jsc is now 35mA/cm^2 , which corresponds to a 10 mA/cm^2 increase in Jsc; when compared to the structure with an AR coating and back reflector only. There is also increased reflectance, due to the out coupling of zero order diffracted or specularly reflected light. However the total reflectance of this structure is just double that of the structure with the AR coating only; the reflectance is plotted in Fig 4.10(a). This grating does wonders for wavelengths near the silicon band edge, as can be observed in Fig 4.10 (b). Further enhancements in absorption can be achieved by varying the geometry of the grating.

This structure culminates this process of addition of components to improve light trapping. From this point forward, we will focus on the specific components and how each can be improved to increase the overall absorption in a solar cell.

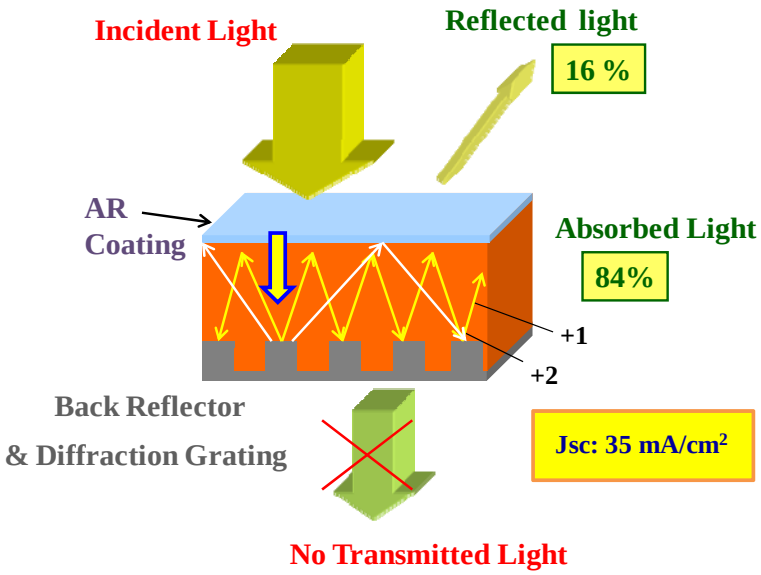

Figure 4.9 Schematic of a plane light wave incident on the surface of silicon with an added AR coating, back reflector and diffraction grating. The grating significantly increases the absorption of light to a value of 84%. Some light gets reflected off the front surface, i.e., double the amount for the structure with AR coating only. The Jsc of this structure is 35 mA/cm^2

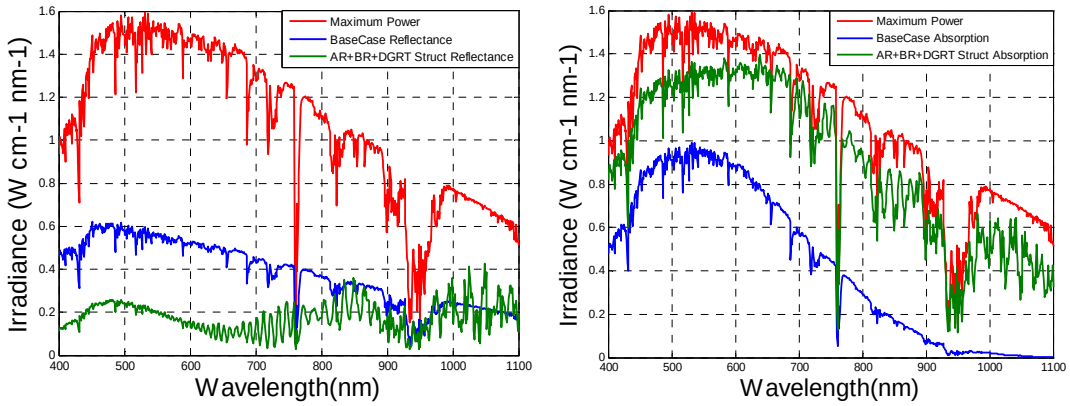

(a) (b)

Figure 4.10 (a) Plot showing the reflectance characteristics of the structure with a back reflector and diffraction grating. In the figure legends, AR+BR +DGRT Struct, corresponds to the structure of Fig. 4.9, (b) the absorption characteristics (green plot), when compared with the incident power (red plot) and bare silicon structure (blue plot) characteristics.

Chapter 5

LIGHT TRAPPING DESIGNS

In chapter 4, we discussed the optics of the light trapping process. In this chapter we follow a similar stream of thought in the design of high efficiency light trapping schemes. The design process is introduced and subsequent results are presented.

5.1 The Design Process

The solar cell structures in consideration incorporate nano scale layers and gratings, in addition, the optical characteristics are calculated for a broad range of wavelengths. As was shown in chapter 4, each specific geometric configuration of design parameters is suited to an individual wavelength. As one can imagine, when you have a broad range of wavelengths, for which each has its own precise design geometry, this becomes an optimization problem. Further, when considering sub-wavelength structures, a rigorous electromagnetic tool is needed to solve for the various fields and effects within the design structure. To this end, we opt to use the scattering matrix (S-Matrix) algorithm as our simulation tool and the particle swarm optimization method, as our optimization algorithm.

The S-Matrix method is advantageous in the analysis of silicon solar cells because of its versatility; it can be used to incorporate lossy (even in metallic materials) and dispersive (frequency dependent) materials. In addition, the S-Matrix method when used

with multiple stacked layers, regardless of the thickness of each layer, is more efficient than volumetric numerical electromagnetic techniques such as the finite element method or the finite difference time domain method.

When the S-Matrix method is applied to grating structures the field along the lateral direction may be expanded using a Fourier series and as a result, the diffraction orders can be easily determined [8], [9]. We also use other electromagnetic modeling tools such as the finite difference time domain method (FDTD) and the rigorous coupled wave analysis (RCWA) to verify the results obtained using the S-Matrix method. More detailed information on the S-Matrix method is available in [8], [9].

For the optimization of design parameters we opt to use the particle swarm optimization (PSO) algorithm which is a population based stochastic optimization technique that derives inspiration from the 'swarming' behavior of various life forms, e.g., a flock of birds [27]. The basic function of the PSO algorithm is as follows: the system is initialized by assigning random population positions and velocities in the problem space. Potential solutions called particles are also initialized in the problem space. The fitness of each individual particle is then calculated. Each particle keeps track of its position in the problem space which is associated with its highest fitness position namely the local best. The best position within all populations is called the global best. So at each time step each particle's velocity is compared to the local best and the global best and then each particle is accelerated towards the local best and the global best positions. We then loop back to the second step, i.e., evaluating the fitness of each individual particle [10], [11].

The equations behind the PSO algorithm can be understood as the changing of the velocity V_i (accelerating) of each particle (entity in the swarm) P_i toward a space of the highest 'fitness' value s_i and the global best, g_i, locations. The basic loop can be summarized using the following equations [10], [11].

$$\begin{aligned} V_{i+1} &= V_i + c_1 rand(s_i - P_i) + c_1 rand(g_i - P_i) \\ P_{i+1} &= P_i + V_{i+1} \end{aligned} \tag{5.1}$$

where *rand()* is a random number generating function that outputs a random value between zero and one.

The PSO algorithm is fast and with few adjustable parameters and therefore finds numerous applications in the optimization of non linear functions [10], [11], [27].

To calculate the fitness of each position in the space we define a figure of merit function; in our analysis we consider two different optimization scenarios. The first is the multiple junction device architecture, and in this case the figure of merit function takes into account both absorption and transmission characteristics at different bandwidths. The absorption is optimized for the 400 – 1100 nm range, and the transmission is optimized for the 1100 – 1800 nm range as shown,

$$\begin{aligned} MF = &\int_{\lambda=400}^{\lambda=1100} [(1 - A(\lambda'))Irrd(\lambda')]^2 + [T(\lambda')Irrd(\lambda')]^2 d\lambda' \\ &+ \int_{\lambda=1100}^{\lambda=1800} [(1 - T(\lambda'))Irrd(\lambda')]^2 + [A(\lambda')Irrd(\lambda')]^2 d\lambda' \end{aligned} \tag{5.2}$$

where A is the absorption, T is the transmission and $Irrd$ is the solar irradiance spectra.

The second scenario considered is the single junction device architecture. In this case the optimization parameter is simply the short circuit current and hence the associated figure of merit is:

$$MF = \int_{\lambda(nm)} \frac{\lambda A(\lambda) Irrd(\lambda)}{1240} d\lambda \tag{5.3}$$

On inspection, one realizes that equation 5.3 is simply the same as that for Jsc (Eqn. 3.1), with all the constants numerically worked out.

With the aforementioned design tools in tow, it is now possible to design high efficiency light trapping structures.

5.2 AR Coating Design and Fabrication

In chapter 4 a mathematical treatment was presented for an ideal AR coating, i.e., at 900 nm. However, in practice, we need to consider the entire spectrum of light that is available to the silicon solar cell when designing the AR coating. In the case of c-Si, since there is a large index contrast between free space and c-Si, the AR coating, hence, consists of multiple layers. The refractive index of free space is taken as 1 and the refractive index of silicon is generally taken to be about 3.5. So, the AR coating materials that apply to c-Si must have refractive indices that fall within the 1 – 3.5 range. There are a number of conventionally used materials in c-Si solar cell AR coatings; these are silicon dioxide (SiO_2), silicon nitride (Si_3N_4) titanium dioxide (TiO_2) and magnesium fluoride (MgF_2).

In our analysis we opt to use a double layer AR coating consisting of SiO_2 with a refractive index of 1.47 – 1.44 in the 400 – 1100 nm range, and Si_3N_4 with an index of 2.08 – 2.01. The structure of the coating has a layer of SiO_2 on top, followed by a layer of Si_3N_4 and finally followed by a thin, 8nm, layer of SiO_2 that is used to passivate the c-Si surface. Optimization results have shown that the optimal design parameters are 99 nm for the SiO_2 layer and 49 nm for the Si_3N_4 layer. The minimal reflectance for this AR coating over the 400 – 1100 nm range of wavelengths is found to be 7.6%.

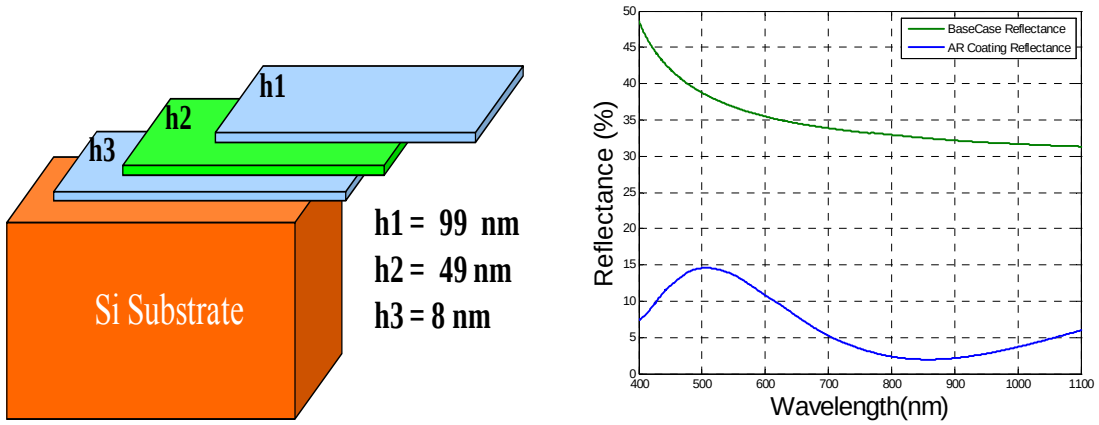

(a) (b)

Figure 5.1 (a) Schematic of silicon solar cell with triple layer AR coating consisting of SiO_2 for h1 and h3, and Si_3N_4 for h2, (b) shows the reflectance characteristics of the solar cell with AR coating, when compared to a bare silicon wafer (referred to as the base case in the figure legend), the reflectance of this structure is 7.6% over the 400 – 1100 nm range.

Equipped with an optimal AR coating design, the next step in the process of design, or device realization, is the assessment of the design viability. To this end, we

endeared to get as realistic designs as possible. The first step in this process was to accurately figure out the optical properties of the various layers included in the design. We hence, deposited individual layers of SiO_2 and Si_3N_4, using plasma enhanced chemical vapor deposition (PECVD). We then employed the use of spectroscopic ellipsometry to accurately obtain the refractive indices and deposition rates of the various materials; c-Si included. All the optical data was fed into the design process material library, i.e., to be used with the S-Matrix tool, and then optimization was performed. We then deposited the layers of optimal thickness onto a c-Si substrate and afterwards measured the layer thicknesses using spectroscopic ellipsometry. Front surface reflectance measurements were then performed using a spectrophotometer equipped with an integrating sphere. This process was repeated in order to figure out fabrication and performance tolerances. Finally we were able to perform a comparative analysis between the simulated and fabricated structures, as is shown in Fig. 5.2. The two matched up very well. Close to the c-Si band edge, the simulated results show pronounced oscillations, these are due to Fabry Perot effects which are accounted for in the simulation algorithm. The spectrophotometer data does not show all these effects due to the normalization procedure performed in acquiring the reflectance data using integrating sphere spectroscopy.

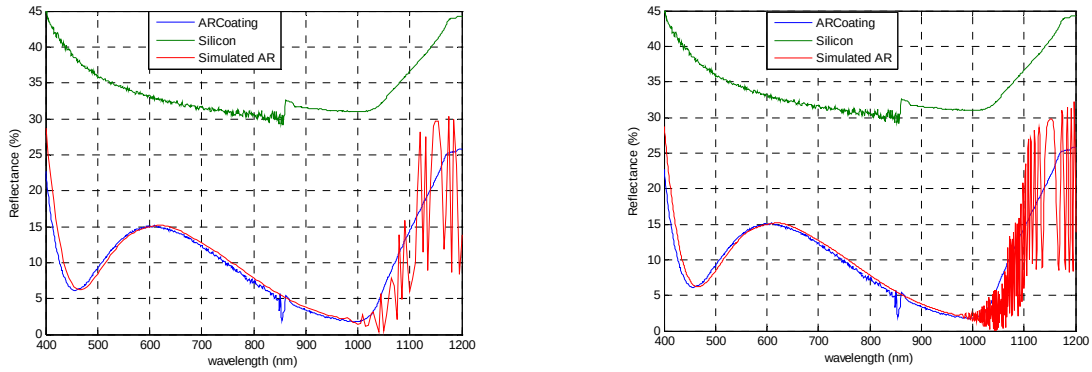

(a) (b)

Figure 5.2 Graphs showing good agreement between fabricated (blue plot) and simulated (red plot) results for reflectance from an AR coating. The green plot shows the measured reflectance of an actual silicon wafer. The simulated data is presented with (a) 5 nm interval and, (b) 1 nm interval. The oscillations near the band edge are due to increased Fabry Perot effects accounted for in the simulation algorithm.

The agreement between simulated and characterization data gives us confidence in the veracity of the design values we achieve using the aforementioned design process.

5.3 High Light Trapping Efficiency Designs

With the design process tools experimentally validated, the next course of action is to consider the apex of light trapping design. The maximal Jsc values achievable with the design structures give us an indication of a feasible upper bound that takes into account factors that have not been considered in the calculation of the theoretical maximum. Such factors include the limits of antireflection and also viable design architecture. With these factors in mind, we set about optimizing the best design structures possible. However, we made a few assumptions in this endeavor, the first being that we considered an ideal reflector as the back reflector material. This assumption lets us ignore, material losses

that are related to reflective materials. Another assumption made was allowing for complicated geometrical structures that are difficult to realize in fabrication, especially with the diffraction gratings.

Binary rectangular gratings are considered because they are easier to fabricate, however, they have a limitation when it comes to light trapping in thin silicon solar cells. In a binary rectangular grating, both positive and negative diffraction orders are reflected from the surface of the grating with the same magnitude. If the diffraction angle is greater than the critical angle, total internal reflection occurs. However, by the reciprocity theorem, the totally internally reflected wave impinges on the surface of the grating in the same way it is generated. Hence, it couples to an outgoing zero order wave that reflects off the surface of the grating and gets lost from the solar cell [20, 26]. To minimize this phenomenon we consider, asymmetric blazed gratings and multiple gratings within the same solar cell structure. When using blazed gratings, we can design them in such a way that zero and negative (left moving) orders are suppressed and hence only positive (right moving) orders remain [26].

To this end, we considered two different designs, the first being a structure with an AR coating and a blazed grating, which we will call High Efficiency Structure 1 (HES 1), as shown in Fig. 5.3 [28]. The optimal design parameters of the grating are shown in Fig. 5.3, with both the period and height of the grating being 800 nm. This structure absorbs 87% of the incident light and has a Jsc value of 36.8 mA/cm^2 . The Jsc characteristics of this design show strong improvement especially close to the silicon band edge, when compared with those of a bare silicon structure as shown in Fig 5.5(a).

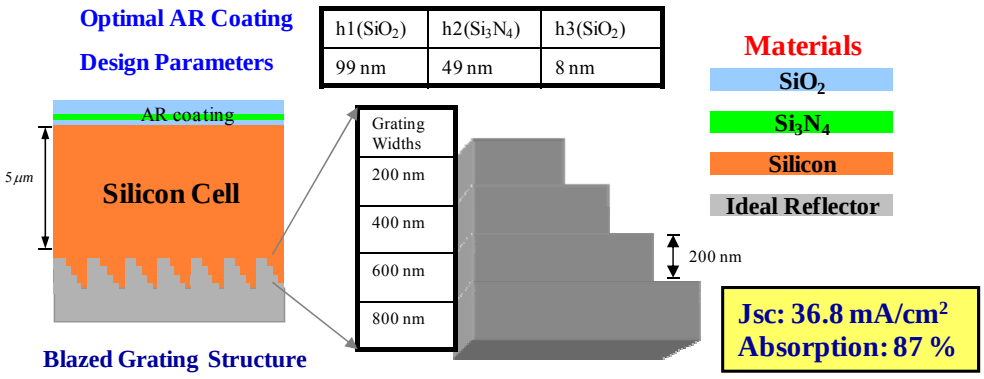

Figure 5.3 Schematic of HES 1; structure with AR coating and Blazed grating. The design parameters of the AR coating and grating are shown, with the grating having both a height and period of 800 nm. The Jsc of this structure is 36.8 mA/cm^2 .

The second high efficiency structure HES 2, incorporates a nano textured top surface and a triangular grating structure [28]. The nano textured top functions as a graded index material for front surface anti reflection, as well as a scatterer of light waves that propagate into the solar cell material. The scattered waves, after propagation through the c-Si structure, fall upon the jagged edged triangular grating where they get diffracted. This architecture has so far proven to yield the highest absorption and Jsc characteristics; the structure has a 90% absorption and a Jsc of 38.51 mA/cm^2 . It is worthy to note that the Jsc value achieved by this HES 2 structure is just 1.19 mA/cm^2 shy of the Jsc value at the geometrical light trapping limit for a 5 micron device; the Jsc limit for a 5 micron device is 39.7 mA/cm^2 . The optimal design parameters are shown in Fig. 5.4. The period of the triangular grating is 560 nm and the height of the grating is 1200 nm. The Jsc characteristics of this design are very impressive with marked increase in Jsc near the band edge, where silicon has poor intrinsic absorption as shown in Fig.5.5 (b).

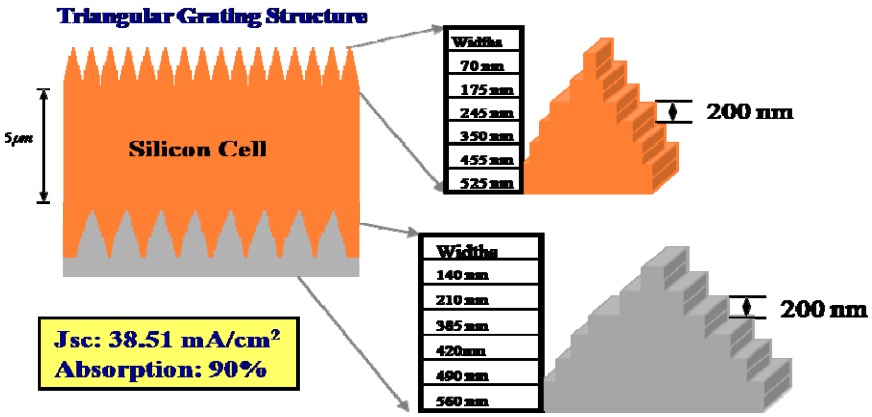

Figure 5.4 Schematic of HES 2 structure that incorporates a nano textured top surface and a triangular grating. The optimal design parameters of the structure are shown, with the grating having an optimal period of 560 nm and a height of 1200 nm.

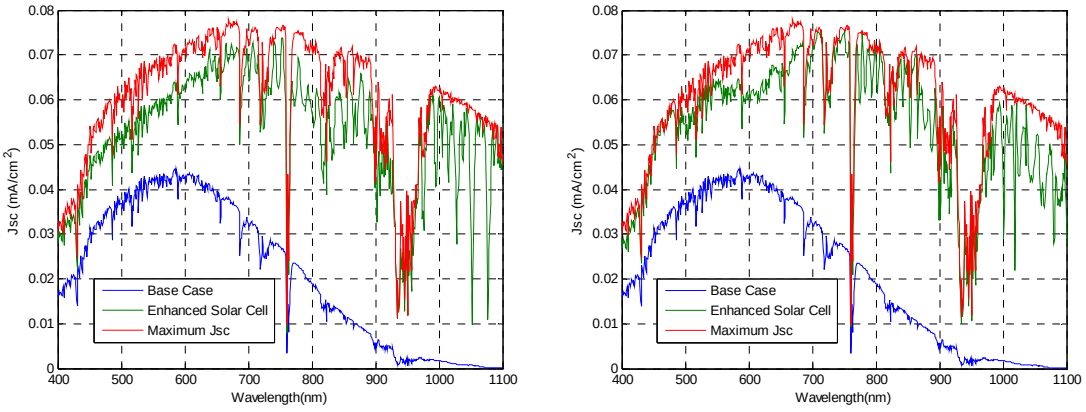

(a) (b)

Figure 5.5 Jsc characteristics of the two HES structures, (a) shows the Jsc characteristics of HES 1 (green plot) as compared to a base case with no light trapping (bleu plot) and the maximum Jsc available (red plot), (b) similarly shows the Jsc characteristics for HES 2 (green plot), with similar color coding to (a).

5.4 Photonic Crystals in Solar Cells

In practice, no structure is ideally reflective over all wavelengths, however it is possible to get a structure that is effective at reflecting at least the band we are most interested in, i.e., close to the silicon band edge. To this end, we introduce a one dimensional photonic crystal (1D-PhC) as a back reflector. A photonic crystal is a periodic arrangement of dielectric or metallic materials with a lattice constant comparable to the wavelength of an electromagnetic wave. The simplest example is a 1D-PhC, where alternating layers of material with different refractive indices are stacked to form a structure that is periodic along one direction. The interaction of an electromagnetic wave with a periodic dielectric structure results in an interference pattern that allows for some light to propagate or be reflected from the different layers of the structure. This phenomenon is described in a band structure, which maps out the range of frequencies that are permitted to propagate and those that are disallowed. The parameters that determine the band structure are the refractive index contrast and thicknesses of the corresponding layers. [20], [29], [30].

One dimensional photonic crystals find many applications including, functioning as high reflectance mirrors and selective light filters. In this thesis, we consider the light selectivity characteristics of the photonic crystal in an attempt to design multi junction device structures. As was mentioned in the introduction chapter, the efforts in this thesis are concerned with designing an efficient light trapping architecture for an element in a multi device stack. In doing this, one has to take into account the performance of

subsequent devices and hence accommodate some of the constraints the situation presents; such as having no back surface reflectors for elements in the stack. To solve this problem we use a 1D-PhC, engineered to reflect and transmit the desired bandwidths. We then cut symmetric and periodic groves into the 1D-PhC layers to form diffractive gratings. This design technique utilizes the beam redirecting property of the grating while still maintaining the selective characteristics of the 1D-PhC [20].

Early work on the incorporation of photonic crystals into solar cells to enhance light trapping was performed by James Gee [31] who put forth the idea that the statistical limit for optical enhancement, shown by Yablonovitch [19] to be $4n^2$ (where n is the refractive index of the material - about 50 for silicon), could be surpassed over a narrow spectral and angular range using photonic band gap materials. More recently several groups have also been working on combining photonic crystals with gratings to enhance the light trapping capabilities of solar cells [32-34]. The novelties of our designs lie in our fundamental approach to designing solar cells that can function both as standalone cells or part of multiple device stacks. We consider the transmission characteristics of the devices to be important and hence we design the photonic crystals to simultaneously reflect shorter wavelengths (400 – 1100 nm) back into the silicon cell and transmit longer wavelengths (1100 – 1800nm) to underlying lower energy cells. In addition, we cut through the layers of the 1D-PhC stack to generate our gratings and are hence able to seamlessly combine the diffractive and reflective properties of the gratings for optimal optical path length enhancement as shown in Fig. 5.6 [20].

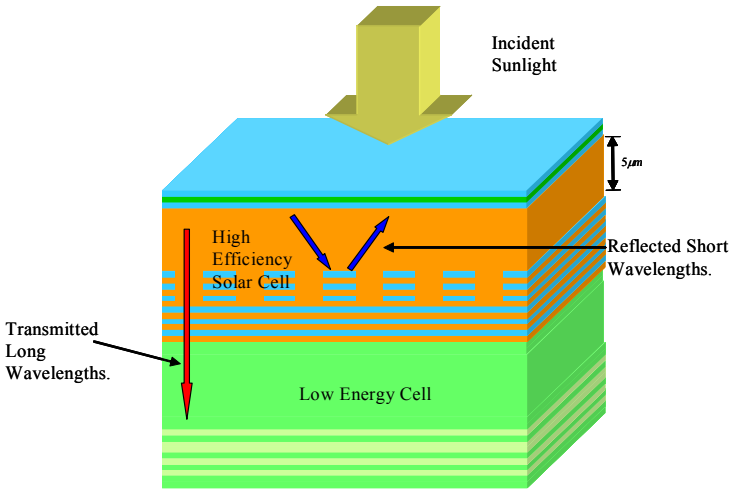

Figure 5.6 Schematic diagram showing a multiple junction solar cell with the short wavelengths being reflected back into the first cell and long wavelengths being transmitted to the lower energy solar cells.

In this study we consider binary and triangular gratings. We choose these gratings because they are relatively easy to fabricate as compared to other grating structures such as blazed gratings. The first design we present includes a triple layer planar AR coating on the front surface and a diffractive binary grating coupled into a 1D-PhC on the back surface; we will refer to this structure as PhC 1. The AR coating consists of a layer of Si_3N_4 embedded between two layers of SiO_2 with the layer nearest the silicon being primarily for the purpose of passivation. The 1D-PhC consists of alternating layers of SiO_2 and amorphous silicon, a-Si. Figure 5.7 (a) is the schematic diagram of the model with an inset scanning electron microscope (SEM) image of the fabricated grating and an inset expanded representation of the grating. The fabrication methodology used to realize the grating is divided into several steps comprised primarily of plasma enhanced

chemical vapor deposition (PECVD), electron beam (E-beam) lithography, and inductively coupled plasma (ICP) etching. The one dimensional photonic crystal layers are deposited by PECVD. The pattern for the diffraction grating in the upper layers of the 1D-PhC is generated using E-beam lithography and transferred with an ICP etching process. Figure 5.7(b) shows the simulated short circuit current characteristics of the designed structure. The enhanced design is compared to a base case that consists of a bare silicon slab with no light trapping and also to the ideal case where the short circuit current is maximum. To optimize the light trapping characteristics we optimized the thicknesses of the AR coating, the alternating photonic crystal layers, and for the grating we considered the period and duty cycle as design parameters. We obtained optimal results for AR coating thicknesses of 98 nm for the top SiO_2 layer and 48 nm for the Si_3N_4 layer with the third SiO_2 layer fixed at 8nm. The optimal grating period is 970 nm, the duty cycle is 0.5 and the thicknesses of the six photonic crystal alternating (a-Si and SiO_2) layers is 128 nm for the SiO_2 layers and 218 nm for the a-Si layers as shown in Fig. 5.7(a). Thus the grating depth is 1038 nm (thickness of three alternating layers); the entire 1D-PhC stack consisted of six alternating layers with the first three etched through to form the grating and the three others placed below the grating. The alternating layer thickness is calculated as an optimization design parameter hence the thickness of layers is the optimal thickness for accomplishing the task of reflecting 400 – 1100 nm light and transmitting 1100 – 1800 nm light [20].

This PhC 1 design augments the reflective and diffractive properties of the grating, which in turn improves the band edge absorption. It absorbs 71 % (400 – 1100

nm) of the incident energy, which results in a short circuit current (400 – 1100 nm) of 27.4 mA/cm^2, a band edge (867 -1100nm) enhancement factor of 3.9 and transmission of 54% of the total energy within the 1100 – 1800 nm wavelength range.

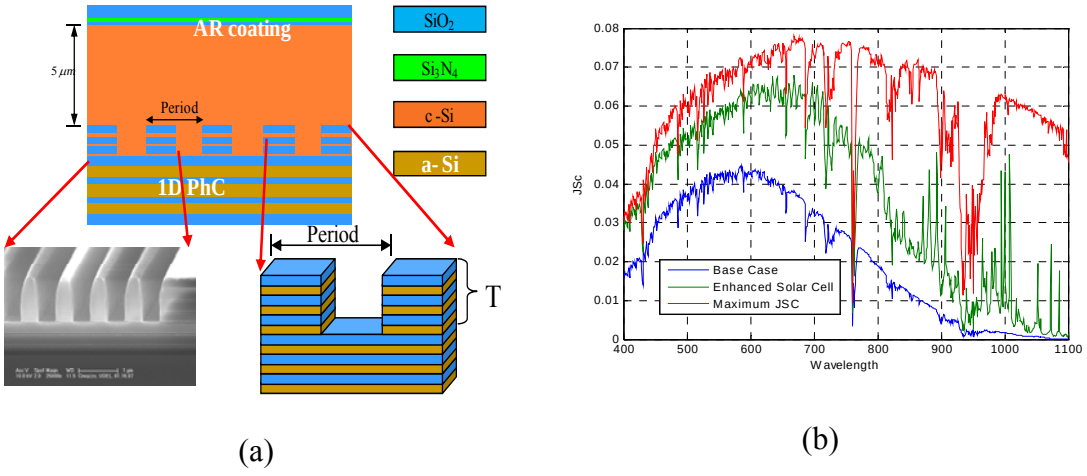

(a) (b)

Figure 5.7 (a) The cross section view of the first solar cell design, PhC 1, with an inset SEM image of the fabricated grating and another showing an expanded view of the grating. The period of the grating is indicated and its value is 970 nm, the thickness of the layers is 128 nm for the SiO_2 layers and 218 nm for the silicon layers, the grating height, indicated as T is 1038 nm and there are 6 alternating layers (each alternating layer consists of a Si and SiO_2 layer) in the entire 1D PhC stack, the grating etches through the first three alternating layers, (b) simulated short circuit current of the designed structure. The Jsc for this structure is 27.4 mA/cm^2.

The second design, PhC 2, as shown in Fig. 5.8(a)., is similar to PhC 1, except that we incorporate a binary grating below the AR coating, which we fill with SiO_2, at the top surface of the cell to introduce diffraction of the incident waves; we also include a triangular grating at the bottom surface. The incorporation of a binary grating at the top of the structure introduces diffraction to the incident wave which is then subject to further

redirection on encountering the triangular grating at the bottom. The combination serves to suppress lower order diffraction modes which are present in PhC 1 and hence further enhances performance. The optimization design parameters are similar to those of PhC 1, with the greatest difference emerging from the introduction of the top grating and multiple periods of the triangular grating. The optimal top grating period is 260 nm and the depth is 280 nm. The alternating photonic crystal layers in the triangular grating had widths of 104 nm for the top alternating layer, 312 nm for the mid layer and 416 nm for the bottom layer of the triangle, as shown in Fig. 5.8(a). The thickness of each of the widths in the grating is 346 nm, i.e., the thickness of an alternating layer (a Si and SiO_2 layer). As with the first structure, the entire 1D-PhC stack consists of six alternating layers with the first three etched through to form the grating and with three others below the grating. The resultant structure proved to be better than the first with 77 % absorption (400 – 1100 nm), a Jsc (400 – 1100 nm) value of 30.25 mA/cm^2, a band edge (867 - 1100nm) enhancement factor of 4.6 and transmission of 41 %(1100 – 1800 nm) [20].

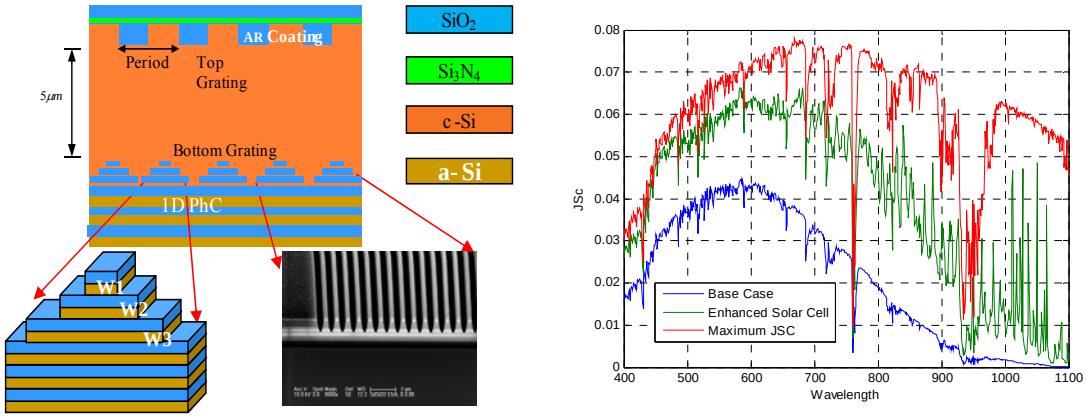

(a) (b)

Figure 5.8 (a) The cross section view of the second solar cell design with an inset SEM image of the fabricated grating and another showing an expanded view of the grating, the grating widths are indicated and the values are W1 = 104 nm, W2 = 312 nm, W3 = 416 nm,(b) the simulated short circuit current characteristics of the designed structure. The Jsc for this structure is 30.3 mA/cm^2

It is interesting to note the added advantage of introducing a top layer binary grating in addition to the symmetric triangular grating; we see an increase in the enhancement factor when compared to PhC 1. Table 5.1 and Fig. 5.9. summarize the performance of our designs when compared, in the 867 – 1100 nm range, to a silicon structure with no light trapping mechanism and one with an AR coating only.

Table 5.1 Enhancement factors for the different devices when compared to a device with no optical enhancements (i.e. no light trapping nor AR coating)

Structure	Enhancement Factor (867 – 1100 nm)
Silicon with no AR coating	1
Silicon with AR coating only	1.4
PhC 1 (with binary grating)	3. 9
PhC 2 (with triangular grating)	4.6

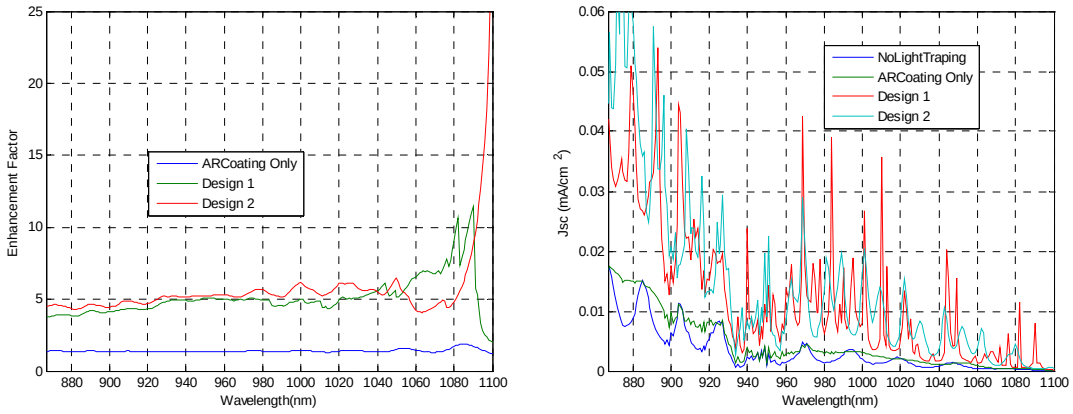

(a) (b)

Figure 5.9 (a) Enhancement factors of the different structures over the wavelength range of 867-1100nm, (b) short circuit current characteristics of the different structures over the wavelength range of 867-1800nm.

Table 5.2 shows the short circuit current values of the different structures and also shows the percentage enhancement of short circuit current, by comparing the Jsc of

enhanced cells to that of a structure with no light trapping or AR coating. This analysis confirms the viability of the enhanced structures as stand alone solar cells because the new designs have high short circuit current values (bandwidth considered is 400 – 1100 nm). We see that in terms of short circuit current the cell performance almost doubles when the double grating (from the second design) is applied i.e. when compared to a cell with no light trapping modifications.

Table 5.2 Short circuit current characteristics and Jsc enhancement of different devices when compared to a device with no optical enhancements (i.e. no light trapping or AR coating)

Structure	Jsc in mA/cm^2 (400 – 1100nm)	Jsc enhancement (Percentage increase) (400 – 1100nm)
Silicon with no AR coating	15.34	N/A
Silicon with AR coating only	21.58	40.6 %
PhC 1 (with binary grating)	27.4	78.5 %
PhC 2(with triangular grating)	30.25	97.2%

Diffraction gratings play a key role in the overall light trapping capabilities of our solar cell structures. In designing these gratings one has to consider three key design parameters, which are: the grating period, the duty cycle and the thickness (height) of the grating. In the binary grating of PhC 1, the duty cycle is fixed at 0.5. The widths of the 1D-PhC layers vary in the case of the triangular grating. The thickness of the gratings in

both the binary and the triangular case are the same because they correspond to the thickness of three alternating layers of the 1D-PhC stack. However, in both cases it is important to analyze the dependence of the cell performance on the period of the gratings. Hence we model the short circuit current characteristics versus the grating period as shown in Fig. 5.10. We analyze grating periods greater than 500 nm because gratings with smaller periods would be more difficult to fabricate on a large scale (we consider 500 -1000 nm). The optimal binary grating period is found to be 970 nm and this corresponds to a Jsc value of 27.4 mA/cm^2 as shown in Fig.5.10 (a). For the triangular grating the optimal period is found to be 520 nm which corresponds to a Jsc value of 30.25 mA/cm^2 as shown in Fig.5.10(b).

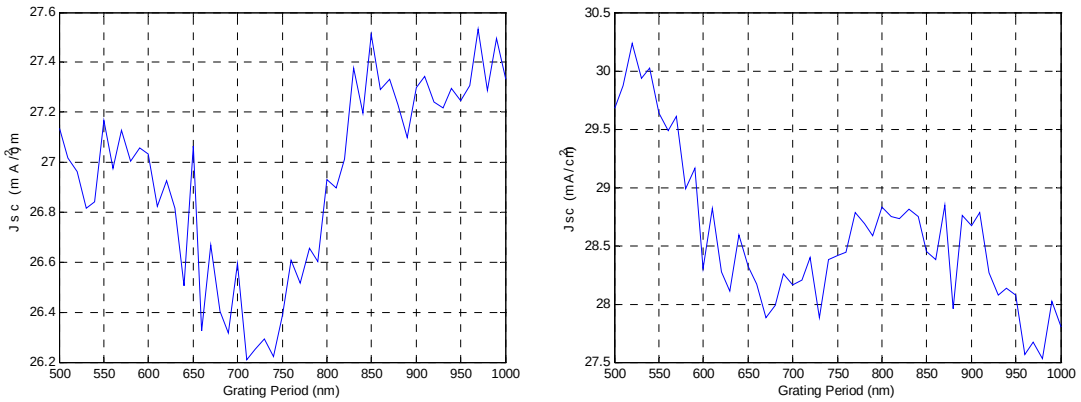

(a) (b)

Figure 5.10 Effect of period on the short circuit current in (a) PhC 1 and (b) PhC 2.

We also consider the effect of variation in the incident angle on the performance of our designs. We observe only slight changes in the short circuit current characteristics

as a result of the different incident angles as shown in Fig. 5.11. The performance of the triangular grating cell actually increases for ten and twenty degree incident angles as shown in Table 5.3; these results illustrate the versatility of the two designs.

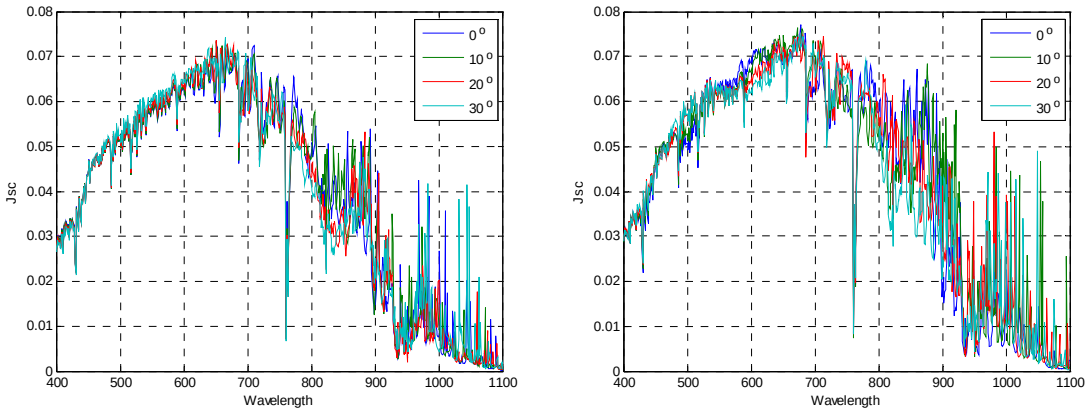

(a) (b)

Figure 5.11 (a) Dependence of cell performance on the angle of incidence of the illuminating light in the cell with a binary grating and, (b) cell with triangular grating. The different incident angles (in degrees) corresponding to the graphs are shown in the figure legends.

Table 5.3 Short circuit current characteristics of PhC 1 and PhC 2 under illumination from light with different incident angles.

Incident Angle (in degrees)	Jsc in mA/cm^2 for PhC 1	Jsc in mA/cm^2 for PhC 2
0	27.4	30.25
10	27.6	30.8
20	27.06	30.6
30	27.3	29.7

Chapter 6

CONCLUSION AND FUTURE WORK

This thesis serves to introduce the fundamental concepts of light trapping and how these concepts can be applied to thin c-Si solar cell devices. The third chapter introduced the light trapping limits and performance metrics used in light trapping analysis. The fourth chapter went further in showing the effects of the addition of various optical light trapping components in an incremental pictorial representation. Concepts such as front surface antireflection, back surface reflectance and diffraction were handled in chapter four.

Chapter five presented the design and analysis of four specific c-Si solar cell structures. The first two structures, HES 1 and HES 2, were designed to show the maximal light trapping limits achievable in the design process. The two structures had high Jsc characteristics with HES 1 having a Jsc of 36.8 mA/cm^2 and HES 2 having a Jsc of 38.51 mA/cm^2 .The Jsc value of HES 2 is just 1.19 shy of the Jsc from a structure at the geometrical light trapping limit for 5 micron devices.

The next two structures PhC 1 and PhC 2, were presented for multi junction solar cell applications. The PhC structures compared the device performance in terms of short circuit current characteristics and the enhancement factor. The highest performance was achieved by the second design, PhC 2, which includes two symmetric gratings, one at the top and one at the bottom of the structure. This second structure, PhC 2, achieves a short

circuit current of 30.25 mA/cm^2 (with normally incident light) and a band edge (867 - 1100nm) enhancement factor of 4.6. We have also shown the SEM images of preliminary fabrication results of the coupled 1D-PhC and diffractive grating nano structures. Our structures achieve the design purpose of absorbing short (400 – 1100 nm) wavelengths, thus improving short circuit current characteristics, while at the same time transmitting longer (1100 – 1800 nm) wavelengths. The 1D-PhC gratings are an effective approach to light trapping in thin film solar cells and hence these structures are viable for both multiple junction and stand alone solar cells. The Jsc and absorption characteristics of the multiple design structures are tabulated in order of increasing performance characteristics in table 6.1.

Table 6.1 Summary of absorption and short circuit current characteristics of the design structures presented in this thesis.

Structure	**Absorption (400 – 1100 nm)**	**Jsc in mA/cm^2 (400 – 1100nm)**
Silicon with no AR coating	40 %	15.34
Silicon with AR coating only	57 %	21.58
PhC 1 (with binary grating)	71 %	27.4
PhC 2(with triangular grating)	77 %	30.25
HES 1 (with blazed grating)	87 %	36.8
HES 2 (with triangular grating)	90 %	38.51
Limit for 5 micron device (Geometric Light Trapping Limit)	92 %	39.7
Maximum Available Power	100 %	43.12

The next course of action, in this study, is the experimental realization of the design structures. To this end, we present a tentative fabrication process in the next section of this chapter.

6.1 Fabrication Process

6.1.1 Thin Film Silicon

We will begin the fabrication of the light trapping structures by first experimenting with each specific component e.g. back surface grating etches on standard 300 micron silicon wafers. Once the process is established, we will begin to experiment with thinner 100 micron wafers; available from University Wafer. We will then extend the process to even thinner off the shelf 50 micron wafers; available again from University Wafer. There are also other vendors who sell ultra thin silicon wafers or silicon on insulator (SOI) wafers, such as SOITEC. All in all, the aim is to establish a process technology that is transferable to a wide variety of thin silicon wafers and also amenable to large scale fabrication processes.

6.1.2 Photonic Crystal and Diffraction Grating Fabrication Process

In this thesis we investigated the optimal design parameters of the photonic crystal diffraction grating periods and found that for the binary grating the value was 970 nm. Since the gratings have a 50% duty cycle, it is experimentally feasible to realize these dimensions in the deep ultraviolet (DUV) regime. Hence, we plan to develop a reverse fabrication process that etches the gratings into the active silicon region after which the photonic crystal layers can be deposited. The process begins by the employment of DUV photolithography to transfer the pattern from a mask, to any photoresist material with

submicron line width control that is suitable for DUV. One such resist is SU-8, a high contrast epoxy based negative photoresist. Although SU-8 is specialized for near UV (350 – 400 nm) processing, recent undertakings in our group have shown that it can be used for DUV (220 nm) lithography with the use of specialized light filters. Hence, the aim would be to develop a reliable DUV lithography process for the fabrication of diffraction gratings.

The SU-8 would act as the photoresist as well as the etch mask, without intermediate transfer steps, which increases the probability of a high yield of quality structures. After the SU-8 is developed, the structure is then ready for silicon etching using a fluorine based ICP. Conventional fluorine based plasma etches are isotropic in nature and hence make it increasingly difficult to control the etch depth, minimize surface roughness and achieve vertical side walls; all of which are critical to the fabrication of accurate diffraction grating structures. To this end, we will leverage the use of a deep reactive ion etching (DRIE) process that is mainly used in the fabrication of 2D photonic crystal structures [35]. This DRIE etch technique increases the anisotropic etching of silicon in the vertical direction, while the etch rate of the sidewalls is decreased by the use of polymer passivation. Polymer passivation is achieved through the addition of gasses like CHF_3 and C_4F_8 (passivant precursors) to the plasma. In conventional etching techniques, all the gases are introduced into the plasma continuously in a gas mixture and hence the deposition of a passivation layer, its removal and etch are carried out concomitantly. This process leads to insufficient sidewall passivation and the formation of undesired surface roughness. To alleviate all the difficulties associated with

conventional techniques we will employ a time multiplexed method that separates the processes of sidewall passivation, trench bottom passivant removal and silicon etching. After etching the diffraction gratings into the silicon, the photonic crystal layers can be deposited by PECVD as shown in Fig. 6.1.

The photonic crystal layers presented in this thesis are mainly optimized for multi junction solar cell technology. Moving forward, we plan on exploring the design space of single junction solar cells and to this end, we plan on exploring methods of increasing the overall reflectance of the photonic crystal. We hence plan on investigating the effects of adding a metallic layer to the back of the photonic crystal structure. In terms of fabrication, after the photonic crystal layer is deposited using PECVD, a metallic layer can be deposited using electron beam (E-beam) evaporation. In the past we have deposited gold, chrome, titanium, silicon, germanium, and silicon dioxide using this method. Electron beam evaporation provides good surface quality thin films that have thicknesses ranging from several nanometers to a few microns.

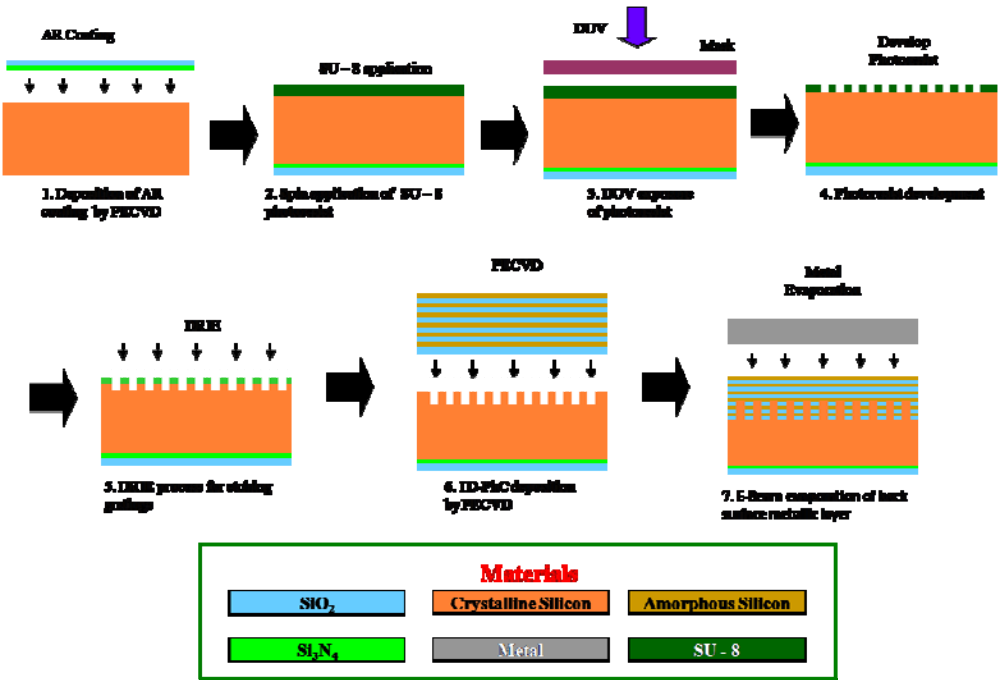

Figure 6.1 Fabrication process (1) AR coating deposition, (2) deposition of SU-8 by spin coating, (3) DUV exposure of mask pattern, (4) photoresist development, (5) DRIE process for etching gratings, (6) 1D-PhC deposition by PECVD, (7) E-Beam evaporation of back surface metallic layer. Inset showing materials used in the process.

6.2 Future Design Concepts

The work presented in this thesis helps to solve a most fundamental optical problem faced by all thin film photovoltaic devices i.e. how to efficiently harness incident sunlight. This problem directly relates to the efficiency of devices, material usage and overall associated costs. The study of employing photonic device engineering techniques to increase light trapping in photovoltaic devices is still in its infancy and there still is much room for exploration in this field. One direction worthy of further exploration is the incorporation of higher dimension photonic crystal structures which can be used to trap

light by taking advantage of their photonic band structure. A photonic crystal can be designed in such a way that normally incident light falls within the pass band (range of frequencies allowed to propagate through the structure) and obliquely incident light falls within the stopband (range of frequencies that do not propagate through structure) of the PhC. We can call such a photonic crystal a specially engineered stopband material (ESBM) and its functionality is illustrated in Fig.6.2.

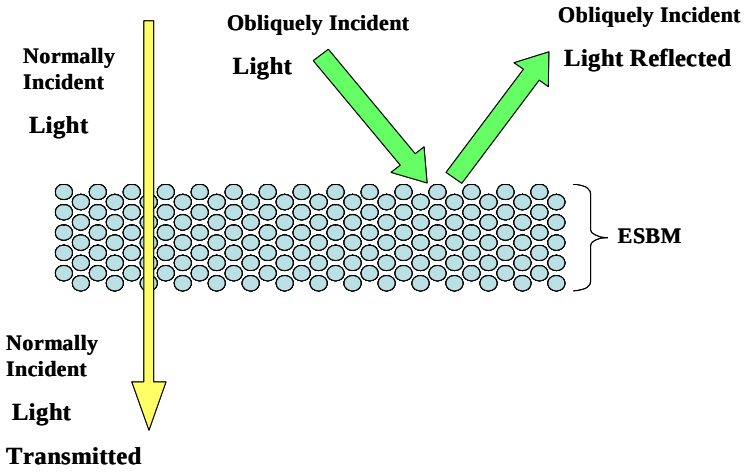

Figure 6.2 Operation of ESBM, normally incident light waves propagate through the ESBM structure while obliquely incident light waves are reflected.

The ESBM structure is directly applicable to the designs described in this thesis, in that it will prevent optical losses that occur due to out coupling of light from the solar cell structures. With the ESBM designed for only normally incident light waves, any diffracted waves which are obliquely incident on the ESBM will be reflected due to the stopband of the structure as illustrated in Fig. 6.3(a) and Fig. 6.3(b). Hence, the total internal reflection conditions occur as a consequence of reflection, or non admittance, of

obliquely incident light waves, rather than primarily on the effects of the refraction of light.

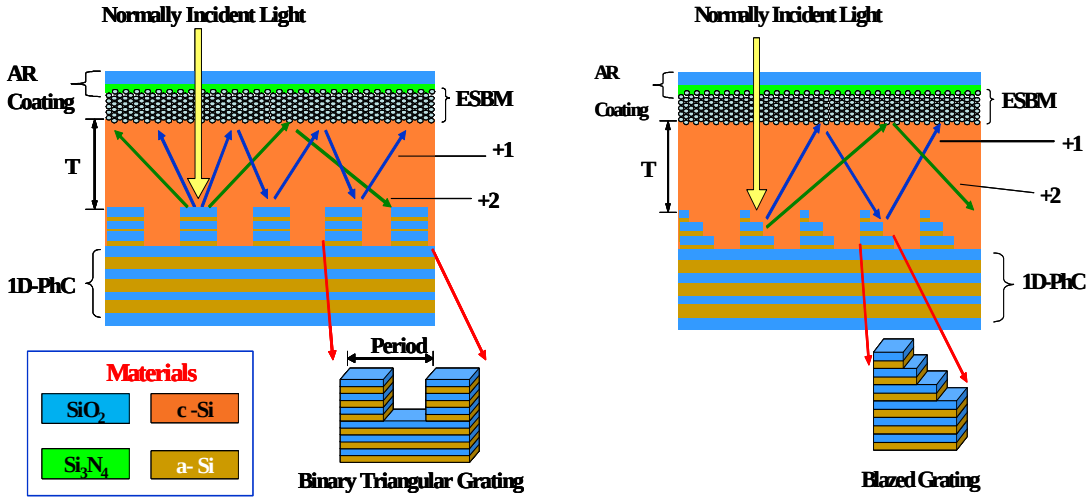

(a) (b)

Figure 6.3 (a) Design of solar cell structure that incorporates an ESBM and binary diffraction grating, (b) second design is a variation of first in that it incorporates a blazed grating for optical path length enhancement. Included in both diagrams is a representation of the different optical path lengths for the first (+1) and second (+2) diffracted orders. The letter T in both designs denotes the thickness of the active silicon layer. This thickness is arbitrary because the designs can be extended to both thin and thick film solar cells.

In the long term the applications of the solar cell designs, presented in this thesis, are varying and far reaching. In the Solar Timeline publication by the Department of Energy (DOE) [36] the expected future directions of solar technology include integration of photovoltaics with building materials, automobiles and even articles of clothing. At the same time DOE predictions indicate competitive pricing of photovoltaic power with traditional sources of electricity in the next few years. Our design technology fits well

into all these endeavors in that the integration of photonic crystals into thin solar cells gives rise to the possibility of integration with glass panels and other building materials.

6.3 Conclusion

The work presented in this thesis helps solve a most fundamental problem faced by all thin film photovoltaic devices, i.e., how to efficiently harness incident sunlight. This problem directly relates to the efficiency of devices, material usage and overall associated costs. The study of employing photonic device engineering techniques to increase light trapping in photovoltaic devices is still in its infancy and there still is much room for exploration in this field.

Thin film solar cell technologies are still yet to reach their full potential, typical efficiencies range from between 5 – 11% for commercial products as opposed to 21% for the best available silicon wafer based modules [37]. In theory, efficiencies of up to 25% are possible for very thin (10 micron) silicon solar cells, however, a stipulation to achieving this great feat is a very high performance light trapping scheme [18, 38][4],[18],[19].

References

[1] B. Obama. (2009, 9). Transcript: Obama's inaugural address. *2009*

[2] B. Obama and J. Biden. New energy for america. *2009*

[3] Catchpole. K. R., M. J. McCann, K. J. Weber and A. W. Blakers, "A review of thin-film crystalline silicon for solar cell applications. Part 2: Foreign substrates," *Solar Energy Materials and Solar Cells,* vol. 68, pp. 173-215, 2001.

[4] R. Brendel and A. Goetzberger, *Thin-Film Crystalline Silicon Solar Cells : Physics and Technology.* Weinheim: Wiley-VCH, 2003, pp. 287.

[5] B. Sopori, "Thin-film silicon solar cells," in *Handbook of Photovoltaic Science and Engineering,* A. Luque and S. Hegedus, Eds. England: John Wiley & Sons, 2003,

[6] A. Barnett, C. Honsberg, D. Kirkpatrick, S. Kurtz, D. Moore, D. Salzman, R. Schwartz, J. Gray, S. Bowden, K. Goossen, M. Haney, D. Aiken, M. Wanlass and K. Emery, "50% efficient solar cell architectures and designs," in *2006 IEEE 4th World Conference on Photovoltaic Energy Conversion, WCPEC-4,* 2007, pp. 2560-2564.

[7] A. Barnett, D. Kirkpatrick and C. Honsberg, "New US ultra high efficiency R&D programme," in *21st European Photovoltaic Solar Energy Conference,* 2006,

[8] A. C. Marsh and J. C. Inkson, "SCATTERING MATRIX THEORY OF TRANSPORT IN HETEROSTRUCTURES," *Semiconductor Science and Technology,* vol. 1, pp. 285-290, 1986.

[9] J. Yonekura, M. Ikeda and T. Baba, "Analysis of finite 2-D photonic crystals of columns and lightwave devices using the scattering matrix method," *J. Lightwave Technol.,* vol. 17, pp. 1500-1508, 1999.

[10] S. Eberhart R. Y., "Particle swarm optimization: Developments, applications and resources," *2001 Congress on Evolutionary Computation,* 2001, pp. 81-86.

[11] R. Eberhart and J. Kennedy, "A new optimizer using particle swarm theory," in *Sixth International Symposium on Micromachine and Human Science,* 1995, pp. 39-43.

[12] C. Honsberg and S. Bowden, "Photovoltaics CDROM,"

[13] M. A. Green, *Solar Cells : Operating Principles, Technology, and System Applications.* Englewood Cliffs, NJ: Prentice-Hall, 1982, pp. 274.

[14] J. Nelson, *The Physics of Solar Cells.* London: Imperial College Press, 2003, pp. 363.

[15] M. J. McCann, K. R. Catchpole, K. J. Weber and A. W. Blakers, "A review of thin-film crystalline silicon for solar cell applications. Part 1: Native substrates," *Solar Energy Materials and Solar Cells,* vol. 68, pp. 135-171, 5. 2001.

[16] K. R. Catchpole, M. J. McCann, K. J. Weber and A. W. Blakers, "A review of thin-film crystalline silicon for solar cell applications. Part 2: Foreign substrates," *Solar Energy Materials and Solar Cells,* vol. 68, pp. 173-215, 5. 2001.

[17] M. A. Green, *Third Generation Photovoltaics : Advanced Solar Energy Conversion.* , vol. 12, Berlin ; New York: Springer, 2003, pp. 160.

[18] M. A. Green, *Silicon Solar Cells, Advanced Principles and Practice.* University of New South Wales: Center for Photovoltaic Devices and Systems, University of New South Wales, 1995,

[19] E. Yablonovitch, "INTENSITY ENHANCEMENT IN TEXTURED OPTICAL SHEETS FOR SOLAR CELLS." in *Conference Record of the 16th IEEE Photovoltaic Specialists Conference - 1982.* 1982, pp. 501-506.

[20] J. G. Mutitu, S. Shi, C. Chen, T. Creazzo, A. Barnett, C. Honsberg and D. W. Prather, "Thin film silicon solar cell design based on photonic crystal and diffractive grating structures," *Optics Express,* vol. 16, pp. 15238-15248, 2008.

[21] C. Balanis, *Advanced Engineering Electromagnetics.* John Wiley and Sons, 1989,

[22] L. Rayleigh, "On the reflection of vibrations at the confines of two media between which the transition is gradual," *Proceedings of the London Mathematics Society,* vol. 11, pp. 51-59, 1879.

[23] J. Müller, B. Rech, J. Springer and M. Vanecek, "TCO and light trapping in silicon thin film solar cells," *Solar Energy,* vol. 77, pp. 917-930, 12. 2004.

[24] H. A. Macleod, *Thin-Film Optical Filters.* ,2.th ed.New York; London: Macmillan; A. Hilger Ltd., 1986, pp. 519.

[25] E. Loewen and E. Popov, *Diffraction Gratings and Applications.* New York, New York: Marcel Dekker Inc, 1997,

[26] C. Heine, "Submicrometer Gratings for Solar Cell Applications," *Applied Optics,* pp. 2476-2482, 1995.

[27] X. Hu, "Particle Swarm Optimization," 2006.

[28] J. G. Mutitu, S. Shi, C. Chen, A. Barnett, C. Honsberg and D. W. Prather, "Light trapping designs for thin film silicon solar cells," in *IGERT: Solar Hydrogen Conference,* 2008,

[29] J. D. Joannopoulos, S. G. .Johnson, J. N. Winn and R. D. Meade, *Photonic Crystals: Molding the Flow of Light.* ,2nd ed.Princeton University Press, 2008,

[30] D. W. Prather, S. Shi, A. Sharkawy, J. Murakowski and G. Schneider, *Photonic Crystals: Theory Applications and Fabrication.* John Wiley and Sons, 2009,

[31] J. M. Gee, "Optically enhanced absorption in thin silicon layers using photonic crystals," in *29th IEEE Photovoltaic Specialists Conference, may 19,2002 - may 24,* 2002, pp. 150-153.

[32] L. Zeng, Y. Yi, C. Hong, B. A. Alamariu, J. Liu, X. Duan and L. C. Kimerling, "New solar cells with novel light trapping via textured photonic crystal back reflector," in *2005 MRS Fall Meeting, November 28,2005 - December 01,* 2006, pp. 251-256.

[33] L. Zeng, Y. Yi, C. Hong, J. Liu, N. Feng, X. Duan, L. C. Kimerling and B. A. Alamariu, "Efficiency enhancement in Si solar cells by textured photonic crystal back reflector," *Appl. Phys. Lett.,* vol. 89, 2006.

[34] P. Bermel, C. Luo, L. Zeng, L. C. Kimerling and J. D. Joannopoulos, "Improving thin-film crystalline silicon solar cell efficiencies with photonic crystals," *Optics Express,* vol. 15, pp. 16986-17000, 2007.

[35] S. Venkataraman, "Fabrication of Two-Dimensional and Tree-Dimensional Photonic Crystal Devices for Applications in Chip-Scale Optical interconnects," 2005.

[36] Department of Energy, "Solar History Timeline," 2009.

[37] M. A. Green, K. Emery, Y. Hishikawa and W. Warta, "Solar cell efficiency tables (Version 33)," *Prog Photovoltaics Res Appl,* vol. 17, pp. 85-94, 2009.

[38] A. V. Shah, H. Schade, M. Vanecek, J. Meier, E. Vallat-Sauvain, N. Wyrsch, U. Kroll, C. Droz and J. Bailat, "Thin-film silicon solar cell technology," *Prog Photovoltaics Res Appl,* vol. 12, pp. 113-142, 2004.